

Tutor/s

Dr. Bernardí Bayarri Ferrer
Departament d'Enginyeria
Química i Química Analítica



Treball Final de Màster

**Removal of micropollutants from wastewater by rice husk biochar:
synthesis, characterisation, and adsorption capacity**

**Eliminació de microcontaminants d'aigües residuals mitjançant
biocarbó de closca d'arròs: síntesi, caracterització i capacitat d'adsorció**

Albert Sales Alba

June 2022



UNIVERSITAT DE
BARCELONA

Dos campus d'excel·lència internacional

B:KC Barcelona
Knowledge
Campus

HUB Health Universitat
de Barcelona
Campus

Aquesta obra esta subjecta a la llicència de
Reconeixement-NoComercial-SenseObraDerivada



<http://creativecommons.org/licenses/by-nc-nd/3.0/es/>

En primer lloc, agrair al meu tutor, el Dr. Bernardí Bayarri, per la confiança dipositada i donar-me l'oportunitat de tornar a treballar de nou dins del grup. Al doctorand Oriol Porcar, per tot el temps que m'ha dedicat i ajudat durant aquest any. A la Dra. Núria López i al Dr. Alberto Cruz, per ser-hi en tot moment quan més ho necessitava i sobretot per transmetre'm les ganes de continuar en la investigació. Donar les gràcies també a l'Ana Piera, que ha estat el meu pilar fonamental dins i fora del laboratori durant aquest any. I a la Laura i l'Adri, per tots els bons moments que hem passat durant aquest semestre. Finalment, agrair per descomptat als meus amics, per tot el suport que m'han donat durant aquesta etapa. I en especial a la meva família, per animar-me sempre a tirar cap endavant i ser una part indispensable de mi. Gràcies a tots.

REPORT

CONTENTS

SUMMARY	iii
1. INTRODUCTION	1
1.1. WATER ISSUES.....	1
1.2. MICROPOLLUTANTS	1
1.3. EUROPEAN WATER POLICY	2
1.4. PESTICIDES.....	3
1.4.1. Neonicotinoids.....	4
1.4.2. Triazines	5
1.5. ADSORPTION.....	7
1.5.1. Adsorption fundamentals	8
1.5.2. Factors affecting the adsorption process.....	9
1.5.3. Adsorption isotherms	9
1.6. ADSORBENT MATERIALS	12
1.6.1. Biochar.....	12
1.6.2. Modified biochar	14
2. OBJECTIVES.....	15
3. MATERIALS AND METHODS.....	17
3.1. CHEMICALS AND REAGENTS	17
3.1.1. Micropollutants.....	17
3.1.2. Other chemicals	17
3.2. WATER MATRIX.....	18
3.2.1. Milli-Q water.....	18
3.2.2. Wastewater samples	19
3.3. BIOMASS MATERIAL	19
3.4. EXPERIMENTAL DEVICES	19
3.4.1. Synthesis and activation of biochar	19
3.4.2. Adsorption experiments.....	20
3.5. ANALYSES	21
3.5.1. Micropollutant concentrations.....	21
3.5.2. Wastewater analysis	21
3.5.3. Biochar characterization.....	23
3.6. EXPERIMENTAL PROCEDURE	27
3.6.1. Synthesis and activation biochar procedure	27
3.6.2. Adsorption experiments.....	27

4. RESULTS AND DISCUSSION	29
4.1. PREVIOUS STUDIES AND CONTROL TESTS	29
4.1.1. Adsorption tests	29
4.1.2. Previous biochar studies	30
4.2. BIOCHAR CHARACTERIZATION	32
4.2.1. Basic properties	32
4.2.2. Proximate analysis.....	33
4.2.3. Surface area, porosity, and physical structure	35
4.2.4. Ultimate analysis.....	37
4.2.5. FTIR spectra	38
4.2.6. Point of zero charge.....	39
4.3. ADSORPTION STUDIES	40
4.3.1. Adsorption at non-constant pH value.....	40
4.3.2. Adsorption mechanism	42
4.3.3. Adsorption isotherms	44
4.4. APPLICATION WITH REAL WASTEWATER	47
5. CONCLUSIONS	51
6. FUTURE PERSPECTIVES	53
7. NOTATION	55
8. REFERENCES AND NOTES	57
APPENDIX	65
APP 1: ADSORPTION PROFILES OF PRELIMINARY EXPERIMENTS	67

SUMMARY

Water is a scarce commodity, continuously exposed to various organic micropollutants, mainly resulting from daily anthropogenic activities. Although these compounds are normally detected in water bodies at very low concentrations, they can also pose a serious threat to the environment and human health. In this regard, pesticides could be considered the micropollutants group with the greatest concern to society.

The adsorption process is recognised as a well-known technique for treating pesticide-contaminated waters. However, conventional adsorbents, such as activated carbon from mineral sources, can still considerably harm the environment. In contrast, biochar is a porous, carbonaceous material resulting from the pyrolysis of biomass in oxygen-depleted conditions. The considerable interest in biochar, mainly due to its remarkable physicochemical properties and its low environmental impact, has led to consider it as a promising alternative adsorbent with great potential in wastewater treatment fields.

The research derived from this work focuses on the synthesis of biochar from rice husk as feedstock, its characterisation, and its evaluation as an adsorbent material capable of removing different pesticides from wastewater.

Biochar was synthesized from pre-treated rice husk feedstock at 500 °C for 4 h under an N₂-H₂ (95:5) atmosphere and, subsequently physically activated by CO₂ at 800°C for 1 h. The resulting biochars, both non-activated and activated, were characterised by several techniques to determine their main physicochemical properties. Both presented high alkaline pH values, high ash content and low carbon, hydrogen, and oxygen percentages. The surface area and morphology confirmed the noteworthy change in biochar surface, from 1.22 to 379.95 m² g⁻¹, upon activation. Moreover, the FTIR spectra confirmed the presence of Si-containing functional groups on activated biochar.

Furthermore, it was also evaluated the adsorption performance of activated biochar in the removal of three pesticides with different n-octanol-water partition coefficients (clothianidin, thiacloprid and atrazine). Using a Milli-Q water matrix and assessing the pesticides adsorption individually, the biochar adsorption trend was firstly clothianidin,

then thiacloprid and finally, atrazine. On the other hand, when they were evaluated simultaneously from the same aqueous solution, biochar exhibited a greater affinity for thiacloprid, followed by clothianidin, and lastly atrazine.

The experimental equilibrium data for thiacloprid and clothianidin was adequately described by the Langmuir model, and the maximum adsorption capacity was quite similar for both, 4068 and 4078 $\mu\text{mol g}^{-1}$, respectively. In contrast, the atrazine adsorption on biochar was reasonably well adjusted by the Freundlich model, indicating also linear adsorption. Furthermore, in all three cases, the effect of pH on pesticide-biochar adsorption was studied and led to the conclusion that electrostatic interactions were not the main mechanism of adsorption in any case.

An experimental study with a real wastewater matrix from a municipal plant was also performed to observe the influence of ions and organic matter on the active sites of biochar. The results evidenced a similar trend of biochar toward clothianidin and thiacloprid, since both achieved around 42-43 % of adsorption at 73 h, whereas for the same time, the adsorption atrazine only was about 23 %. In contrast, for the same conditions but with milli-Q water, the three pesticide adsorption was almost complete within approximately 30 h.

In conclusion, the outcomes indicated that CO₂-physically activated biochar from rice husk biochar can be used as a readily available adsorbent for the removal of clothianidin, thiacloprid and atrazine from contaminated water, both individually and simultaneously.

Keywords: Adsorption, Atrazine, Biochar, Clothianidin, Thiacloprid, Wastewater

1. INTRODUCTION

1.1. WATER ISSUES

Water resources are essential to human life, socio-economic development, and ecosystem health. During the past several decades, human water withdrawal has increased considerably, mainly due to rapid population growth and rising living standards (Huang et al., 2021). According to the World Wildlife Fund (WWF) estimations, at the current water consumption rate, in 2025 two-thirds of the world population could face water scarcity (López-Vinent et al., 2021). Furthermore, other issues, such as climate change are also expected to considerably reduce water availability in the future (Rafiei-Sardooi et al., 2022).

To minimize this backdrop, providing an adequate quantity and quality of water is a main objective of the global water community. It is enshrined in Goal 6 of the United Nations (UN) Sustainable Development Goals (SDGs): Ensure availability and sustainable management of water and sanitation for all (Gleick & Cooley, 2021). Specifically, SDG Target 6.3. states: *“By 2030, improve water quality by reducing pollution, eliminating dumping and minimizing release of hazardous chemicals and materials, halving the proportion of untreated wastewater and substantially increasing recycling and safe reuse globally”* (UN General Assembly, 2015).

1.2. MICROPOLLUTANTS

Micropollutants (MPs) are natural or synthetic organic compounds, resulting from daily anthropogenic activities, mainly detected in the surface and groundwater at trace levels, from a few ng L⁻¹ to several µg L⁻¹ (Sousa et al., 2019). In recent decades, the widespread presence of many such substances has become an increasingly global environmental concern. Despite their low concentrations in water bodies, conventional wastewater treatment plants (WWTPs) cannot warrant the complete removal of these complex substances, leading to their continuous introduction into the environment, where they can cause serious toxic and allergenic effects on living organisms (Serrano et al., 2019).

Micropollutants can be divided into six major groups: pharmaceuticals, personal care products, steroid hormones, surfactants, industrial chemicals, and pesticides (see Figure 1) (Luo et al., 2014).

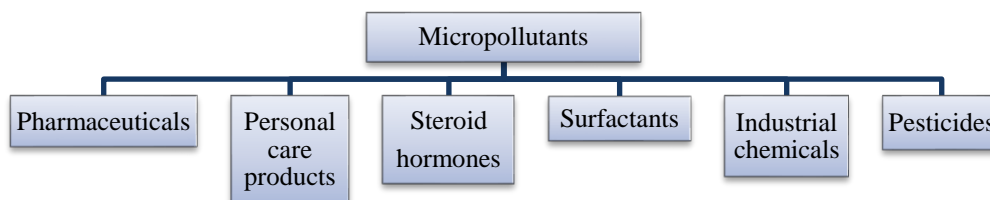


Figure 1. Categories of micropollutants in the aquatic environment (Luo et al., 2014).

Due to the potential risks of these substances, linked to their presence in natural waters and their resistance to conventional wastewater treatments, numerous micropollutants have been also labelled as contaminants of emerging concern (CECs). Even though the names are commonly used interchangeably, CECs are not subject to any water quality regulations, while MPs may have previously been regulated and included as priority substances (PSs) in related legislation (Cruz Alcalde, 2020).

1.3. EUROPEAN WATER POLICY

The European Union Water Framework Directive (EU WFD, 2000/60/EC) was a significant milestone in the European water policy and has served as the legal basis for the EU Members States to protect their freshwater bodies, both surfaces and groundwater (Barbosa et al., 2016; Weisner et al., 2022). A main goal of the EU WFD was to monitor certain chemical pollutants, known as priority substances, and ensure that they do not exceed specific concentration thresholds in surface water, the so-called Environmental Quality Standards (EQSs) (Pesqueira et al., 2020; Tiedeken et al., 2017). In 2008, Directive 2008/105/EC finally ratified a total of 33 priority substances and their respective EQS (Barbosa et al., 2016).

Directive 2013/39/EU updated the above-mentioned directives, recommending the monitoring of 45 PSs (12 organic compounds and 4 metals were added to the earlier list) and highlighted the demand to develop new water treatment solutions (Sousa et al., 2019). Furthermore, Directive 2013/39/EU also led to creating a Watch List (WL) of substances that were not routinely monitored but which might pose a significant risk

due to potential toxicological effects when presented in water bodies. The full list was published in the Decision 2015/495/EU (Pesqueira et al., 2020). The compounds included in it had to be monitored Europe-wide to gather data on their occurrence in water bodies. Based on the information collected, a risk assessment had to be carried out, and the Watch List compounds might be included in the PSs list, thereby adopting the consequent EQS (Gusmaroli et al., 2019).

In June 2018, the second updated version of the EU Watch List was published by Decision 2018/840/EU. Most of the compounds present in the first are still characterized due to insufficient monitoring data to perform a proper risk assessment. Consequently, many have also been included in the second release (Gusmaroli et al., 2019). The 2nd Watch List includes 15 CECs: 7 pesticides, 5 pharmaceuticals and 3 steroid hormones (Jurado et al., 2019).

1.4. PESTICIDES

Approximately half of the compounds included in the 2nd Watch List (7 out of 15) and PSs list (23 out of 45) are pesticides. It represents around 50 % of the overall European priority and emerging concern substances, which is not a coincidence given the nature of these compounds (Cruz Alcalde, 2020).

According to the World Health Organization (WHO), pesticides are chemical compounds used to kill pests, including insects, rodents, fungi, and weeds. They play a significant role in the public health and agricultural sectors, controlling disease vectors and crop pests (Rezende-Teixeira et al., 2022). Based on the United Nations Food and Agriculture Organization (UN-FAO) statistics, around 4.16 million tonnes of pesticides were employed in agricultural use in 2019 globally. Asia and the Americas were the top and second-largest pesticide users in 2019, 51.5 % and 32.7 %, respectively. Regarding the EU, pesticide use in the same year represented about 8.35 %. (FAO, 2022).

With the increasing use of pesticides in modern agriculture, the variety of pesticides has become even more diverse. Based on their target organisms, pesticides can be divided into insecticides, herbicides, fungicides, nematicides, and avicides (Liang et al., 2022).

1.4.1. Neonicotinoids

Neonicotinoids (NNs), also known as neonics, are currently the most widely consumed insecticides worldwide. They were introduced to the global market in the early 1990s, and by 2010, seven major neonicotinoid compounds represented about one-third of the global insecticide market (Sgolastra et al., 2020). Their fast-growing popularity is mainly related to their versatility of use, high efficacy, long persistence, and systemic nature (Naumann et al., 2022).

Neonicotinoids are derived from nicotine, so they can bind strongly to nicotinic acetylcholine receptors (nAChRs) in the central nervous system of insects, causing nervous stimulation at low concentrations, but receptor blockage, paralysis, and even death at high concentrations (Goulson, 2013; Li et al., 2018). Recent studies reveal that these insecticides can also cause adverse effects on invertebrate and vertebrate non-target organisms (Pietrzak et al., 2020). Moreover, chronic exposure to them may provoke certain types of developmental disorders in human health (Cruz-Alcalde et al., 2017). It was also shown that neonicotinoids indirectly reduce fish and bird populations by disrupting their food webs (Naumann et al., 2022).

This class of insecticides are small molecules with high water solubility and low volatility, hence their high potential to leach into surface or underground waters, being one of the current worldwide concerns about the extensive use of neonicotinoids (P. Zhang, Ren, et al., 2018; P. Zhang, Sun, et al., 2018).

Clothianidin

Clothianidin (CTD), as the second generation of neonicotinoids, is currently one of the most known and available neonic insecticides on the agrochemical market (Fierascu et al., 2020; C. Zhang et al., 2020). The structural features of clothianidin (see Table 1) are an open-chain N-nitroguanidine skeleton and a chloro-thiazole ring. This chemical compound is moderately soluble in water (327 mg L⁻¹ at 20 °C) and presents low hydrophobicity (log K_{ow} = 0.7) and a pK_a value of 11.09.

This neonicotinoid pesticide is currently on the 2nd WL for monitoring in water bodies. However, due to the risk clothianidin also poses to pollinators, especially honeybees, its use on open field crops was banned in 2018 by the EU through Implementing Regulation (EU) 2018/784. Hence, its usage is now only authorised in permanent greenhouses (European Commission, 2018).

Thiacloprid

Thiacloprid (TCP) is also a second-generation neonicotinoid insecticide widely used in modern agriculture to control hymenopterous insects and, over the last decades, has become one of the most concerning contaminants (Yang et al., 2022). Thiacloprid (see Table 1) has three important biologically active groups in its structure: chloro-pyridine and thiazolidine rings and the cyanoimino group. This chemical compound also has very high stability and moderate solubility in water (185 mg L⁻¹ at 20 °C). Furthermore, thiacloprid presents a low octanol-water partition coefficient ($\log K_{OW} = 1.26$) and does not dissociate in aqueous solutions.

Regarding honeybees, the N-cyanoimine neonicotinoids (thiacloprid) have considerably lower toxicity than the N-nitroimine neonicotinoids (clothianidin). However, in 2020, the EU by Implementing Regulation (EU) 2020/23 did not renew the approval of the active substance thiacloprid, as it cannot be proven that the presence of thiacloprid metabolites in groundwater will not lead to unacceptable effects on groundwaters and harmful effects on human health (European Commission, 2020). Moreover, this neonic pesticide is still on the 2nd WL for monitoring in water bodies.

1.4.2. Triazines

Triazines are a group of herbicides that presents a substituted heterocyclic ring structure composed of a C₃H₃N₃ moiety. They are considered among the most important classes of pesticides (Manousi et al., 2022). According to the arrangement of the nitrogen atoms, exist three triazine isomers: 1,2,3-triazine 1,2,4-triazine and 1,3,5-triazine. The latter, which is probably the most common form, is also known as symmetric triazines (s-triazines) (Chauhan et al., 2021).

The action mechanism of s-triazine herbicides is based on the inhibition of photosynthesis, as they can bind to the QB protein in the photosystem II reaction centre and block the flow of electrons through the photosynthetic electron transport chain (Semren et al., 2018).

Atrazine

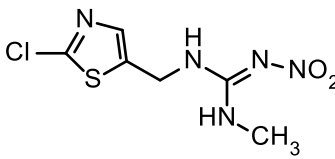
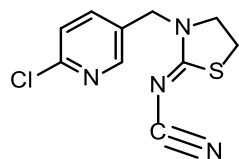
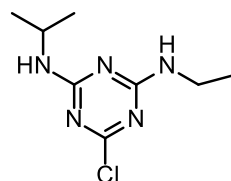
Atrazine (ATZ) is a herbicide from the s-triazines group, widely used in corn and sugar cane crops, being extensively spread worldwide due to its high effectiveness in combating weeds (Salomón et al., 2022). This chemical compound is represented by a triazine ring substituted with a chlorine, ethylamine and isopropylamine group (see Table 1). It also presents a low water solubility (34.7 mg L⁻¹ at 26 °C), a moderate hydrophobicity (log *K*_{OW} = 2.61) and a p*K*_a of 1.70 (Aldeguer Esquerdo et al., 2021).

Due to its structural stability, long residual period and non-biodegradable properties, atrazine could persist for a long time after being transported to surface and groundwaters, which would harm water quality and ecosystems (Jiang et al., 2020). Atrazine is also classified as Group 2B by International Agency for Research on Cancer (IARC), meaning that it is possibly carcinogenic to humans (Phan et al., 2022). Moreover, according to the risk assessment report of the US Environmental Protection Agency (EPA), atrazine could have some harmful impact on fish, terrestrial and aquatic plants, and it might also adversely affect reptiles and amphibians (He et al., 2019).

In 2004, atrazine was not included in the EU list of authorised products, owing to its significant risk of contaminating groundwaters (European Commission, 2004). However, it is still widely used in agriculture in other countries, such as the United States, Brazil, China, and India (de Albuquerque et al., 2020).

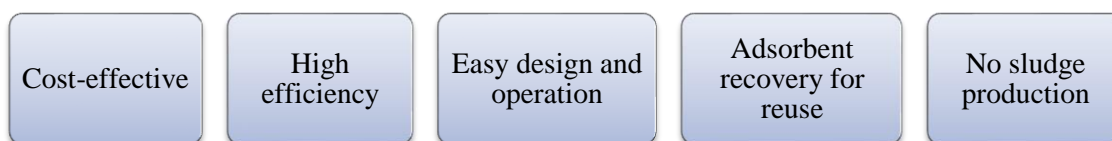
Atrazine is one of the 45 substances listed in the Directive 2013/39/EU on water policy as priority water pollutants. In addition, in terms of water quality for human consumption, the EU, by Directive 2020/2184/EU, set the maximum allowable atrazine level for drinking water at 0.1 µg L⁻¹, while the WHO established at 2 µg L⁻¹ (Steffens et al., 2022).

Table 1. Compound names, solubility in water values, octanol-water partition coefficients and chemical structures of pesticides clothianidin, thiacloprid and atrazine.

Compound name	Solubility in water (mg L ⁻¹)	Log K _{ow}	Chemical Structure
Clothianidin	327	0.70	
Thiacloprid	185	1.26	
Atrazine	34.70	2.61	

1.5. ADSORPTION

Several techniques are available for pesticide removal from aqueous solutions, which can be classified into biological, chemical, and physical processes. Examples of these treatment technologies include advanced oxidation processes (AOPs), photocatalysis, biodegradation, membrane techniques, filtration, and adsorption (Mondol & Jung, 2021; Saleh et al., 2020). Among them, adsorption presents superior advantages (see Figure 2) over some other methods for removing contaminants at low concentrations (V. S. Tran et al., 2015). Nevertheless, the adsorption process also presents some drawbacks, including the high cost of typical adsorbents.

**Figure 2.** Advantages of the adsorption process (Sharifi et al., 2022).

1.5.1. Adsorption fundamentals

Adsorption is a surface phenomenon in which a solution containing an adsorbable solute (adsorbate) meets a solid with a highly porous surface structure (adsorbent). The liquid-solid intermolecular attraction forces drive some solute molecules from the solution to concentrate or deposit on the solid phase surface, thus decontaminating the liquid phase (Nageeb, 2013). The opposite process, namely the detachment of an adsorbate molecule from the adsorbent surface, is generally known as desorption.

The adsorption process on an adsorbent from the aqueous phase involves the following steps: i) mass transfer of the solute by diffusion from the bulk fluid phase to the solid external surface (film diffusion), ii) mass transfer of the adsorbate by internal diffusion into the adsorbent pores and the adsorbed phase (intraparticle diffusion), and iii) adsorption of the adsorbate on active sites of the solid (Girish & Murty, 2016).

Depending on the interactions between the solid phase surface and the adsorbate in the last step, the adsorption process can be classified as physical adsorption (*physisorption*) or chemical adsorption (*chemisorption*).

Physisorption is due to relatively weak attractive forces, involving mainly van der Waals interactions, supplemented in many cases by electrostatics contributions. Multilayers are generated on the adsorbent surface in this fast and reversible method (de Gisi et al., 2016; Rathi & Kumar, 2021).

In contrast, chemisorption is due mainly to chemical bondings. It is a slower method, only generates a monolayer, and occurs at temperatures higher than the critical temperature of the adsorbate. Under favourable conditions, both processes can occur simultaneously or successively (de Gisi et al., 2016; Rathi & Kumar, 2021).

In general, the adsorption mechanism of organic compounds, such as pesticides, on biochar (see Figure 3) can be mainly explained by pore-filling, hydrogen bonding formation, hydrophobic effect, electrostatic reactions, and electron donor-acceptor (EDA) interactions (Ambaye et al., 2021; X. Wang et al., 2020).

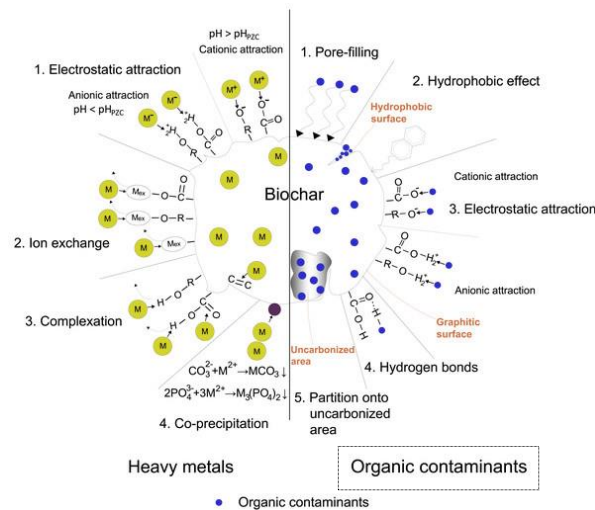


Figure 3. Adsorption mechanisms of heavy metals and organic contaminants on biochar (X. Wang et al., 2020).

1.5.2. Factors affecting the adsorption process

Different variables should be considered when studying an adsorption process since they can considerably influence it. Adsorption performance is primarily influenced by physicochemical factors (see Figure 4) and adsorbent properties. Furthermore, some consideration must also be given to adsorbate characteristics, such as its weight, structure and molecular size, its octanol-water coefficient and polarity (Rápó & Tonk, 2017). Further explanation about how these variables can affect the process will be introduced during the discussion of the results.

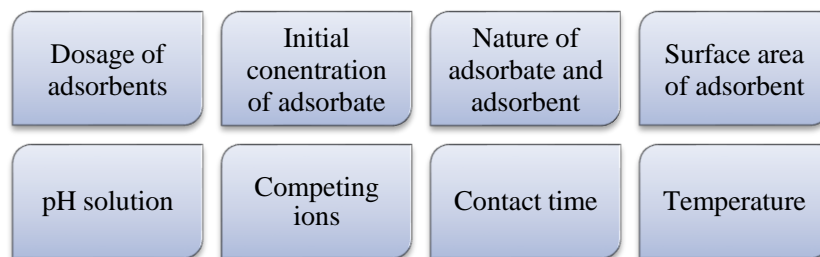


Figure 4. The main factors affecting the adsorption process (Rathi & Kumar, 2021).

1.5.3. Adsorption isotherms

Adsorption isotherms are the presentation of the amount of adsorbed solute per unit of adsorbent weight as a function of the equilibrium concentration in the bulk solution, under thermodynamic equilibrium conditions (Nageeb, 2013). To select a model that describes well the adsorption system, the experimental data are used to generate the

different isotherm profiles (see Figure 5). The isotherm model which best fits the isotherm profile is chosen as an equilibrium representation of the adsorption system (Yousef et al., 2020). The so-called Langmuir and Freundlich isotherms are the most commonly used adsorption models.

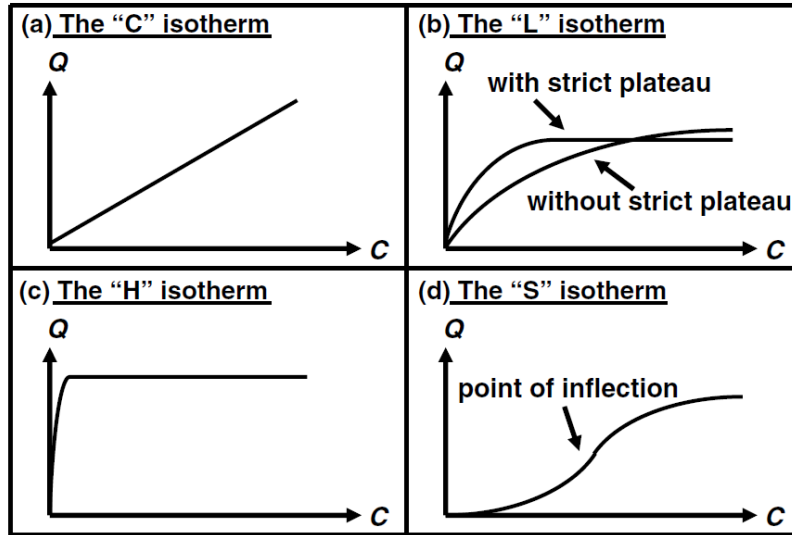


Figure 5. The four main types of isotherms profiles (Limousin et al., 2007)

Langmuir isotherm model

The Langmuir model (1918) is one of the oldest empirical methods used to describe the adsorption isotherms. It assumes monolayer adsorption onto a homogeneous surface, containing a finite and fixed number of adsorption sites available of uniform energies and that there is no interaction between the adsorbed species (Salman et al., 2011). The Langmuir isotherm (Piccin et al., 2011) can be described by Equation (1).

$$\frac{C_e}{q_e} = \frac{1}{K_L \cdot q_m} + \frac{C_e}{q_m} \quad (1)$$

Where C_e is the equilibrium concentration of solute ($\mu\text{mol L}^{-1}$), q_e is the amount of adsorbed solute per unit weight of adsorbent ($\mu\text{mol g}^{-1}$), also known as adsorption capacity, K_L is the Langmuir constant ($\text{L } \mu\text{mol}^{-1}$), which is related to adsorption energy and capacity, and q_m is the maximum monolayer adsorption capacity ($\mu\text{mol g}^{-1}$).

Langmuir isotherm is characterized graphically by a plateau, an equilibrium saturation point at which no further adsorption can occur after a molecule occupies a site (Foo & Hameed, 2010). Therefore, according to Figure 5, it would be classified within the "L"

type isotherms. The essential characteristics of the Langmuir isotherm model can be expressed in terms of a dimensionless constant, known as the separation factor (R_L) and represented by Equation (2) (H. N. Tran et al., 2017).

$$R_L = \frac{1}{1 + K_L C_o} \quad (2)$$

Where K_L is the Langmuir equilibrium constant ($L \mu\text{mol}^{-1}$), and C_o is the initial adsorbate concentration ($\mu\text{mol g}^{-1}$). R_L value indicates the adsorption process to be unfavourable ($R_L > 1$), linear ($R_L = 1$), favourable ($0 < R_L < 1$), or irreversible ($R_L = 0$) (Ayawei et al., 2017).

Freundlich isotherm model

The Freundlich isotherm (1906) is the oldest known model which considers the non-ideal and reversibility of the adsorption process. Unlike the Langmuir, the Freundlich isotherm model is based on multilayer adsorption on a heterogeneous surface, with a non-uniform distribution of adsorption heat and affinity (Yousef et al., 2020).

The nonlinear form of the Freundlich equation (H. N. Tran et al., 2017) can be expressed as shown in Equation (3).

$$q_e = K_F C_e^n \quad (3)$$

Where q_e is the amount of adsorbed solute per unit weight of adsorbent uptake at equilibrium ($\mu\text{mol g}^{-1}$), C_e is the equilibrium concentration of solute (mmol L^{-1}), K_F is the Freundlich constant ($\mu\text{mol g}^{-1}/(\mu\text{mol L}^{-1})^n$), also related to adsorption capacity, and n (dimensionless) is the Freundlich intensity parameter. The exponent n is related to the energetic heterogeneity of the adsorbent surface and determines the curvature of isotherms: favourable ($n < 1$), linear ($n=1$) or unfavourable ($n > 1$) (Eckhard Worch, 2012).

According to the Freundlich equation, this isotherm, which is also part of the "L" isotherms, does not reach a plateau with increasing concentration since the solid clearly does not show a limited sorption capacity (Limousin et al., 2007).

1.6. ADSORBENT MATERIALS

Selecting, developing, and characterizing the adsorbent material is an essential point for correctly designing an adsorption process for any application. Focusing on water treatment applications, some characteristics that a proper adsorbent must present are good chemical and mechanical stability, low cost and availability, and especially excellent surface and physicochemical characteristics. So, in this way, the adsorbent shows a higher adsorption capacity, with a faster kinetic, thus achieving a higher overall efficiency (Dotto & McKay, 2020).

Adsorbents can be classified into natural adsorbents, either organic or inorganic, and synthetic adsorbents. The main natural adsorbents include clays, minerals, zeolites, and charcoal, while synthetic adsorbents are prepared from different types of waste, whether from agricultural, industrial, or household activities (Nageeb, 2013).

Activated carbon (AC), a material mainly derived from charcoal, is recognized as one of the most popular and widely used adsorbents in the water and wastewater treatment processes (Justo Llopis, 2015) because its large surface area, considerable microporosity and high adsorption capacity (Vinayagam et al., 2022). However, this typical adsorbent presents some compelling problems related to its high associated costs, regenerative capacity, and end-of-life disposal (Ponnuchamy et al., 2021). Over the past few years, researchers have mainly focused on the development of new cost-effective and environmentally friendly adsorbents for industrial applications, such as biochar (BC).

1.6.1. Biochar

Biochar is generally defined as a porous, carbonaceous material produced by thermal conversion of biomass, either from vegetal and/or animal origin, in an oxygen-depleted atmosphere (Phuong et al., 2016). There are diverse thermal conversion techniques, such as pyrolysis, gasification, torrefaction, and hydrothermal carbonization. Depending on its residence time and temperature, pyrolysis can be divided into flash, fast and slow pyrolysis. From these techniques, slow pyrolysis seems to be the most cost-effective and efficient method for biochar production (see Table 2) (Varjani et al., 2019).

Table 2. Characteristics of pyrolysis processes (Nidheesh et al., 2021; C. Wang, 2021)

	Slow pyrolysis	Fast pyrolysis	Flash pyrolysis
Temperature (°C)	300 – 700	500 – 1000	900 - 1200
Residence time	minutes to hours	seconds to minutes	few seconds
Heating rate (°C/s)	0.1 – 1	10 – 200	> 1000
Biochar yield (%)	35 – 50	15 – 35	10 – 20

Reaction conditions such as pyrolysis temperature, residence time, and heating rate play a key role in biochar synthesis. Among these three parameters, pyrolysis temperature is probably the most significant factor since it affects the structural characteristics, morphology, and aromaticity, also known as the H/C atomic ratio. The carbonization degree and the production of biochar are mainly influenced by residence time, whereas the heating rate might impact biochar stability (R. Z. Wang et al., 2019). In addition, the feedstock type, and its properties such as the structure, shape, size, and chemical composition (lignocellulosic compounds and minerals contents) can also considerably influence physicochemical and structural changes in the biomass during the pyrolysis process. It determines many characteristics of the resulting biochar: ash and moisture content, fixed carbon and volatile components fractions, pH, surface area, elemental composition, and porosity, among others (Nartey & Zhao, 2014; Yavari et al., 2017).

Biochar receives much interest as a soil amendment because of its carbon sequestration potential and its ability to minimise the climate change effects. However, over the last decade, it has been gaining more ground to use biochar as an alternative adsorbent for the removal of pollutants from aqueous solutions (Chemerys & Baltrėnaitė, 2016). Such interest stems mainly from the outstanding properties biochar can achieve, such as a large specific surface area (SSA), well-developed pores, a high amount of surface functional groups, significant resistance to mineralization and polyaromatic carbons compositions (Nzediegwu et al., 2022; Yavari et al., 2017). Nevertheless, to acquire these desired properties, several experimental studies have revealed the need to modify biochar and hence improve the overall adsorption performance (Qiu et al., 2021).

1.6.2. Modified biochar

In recent years, researchers have proposed diverse methods for biochar modification. This procedure can be generally undertaken in two forms. The first one is based on the modification of the raw materials used to prepare biochar (pre-pyrolysis modification), whereas the second one involves only modifying the resulting biochar (post-pyrolysis modification) (Qiu et al., 2021). The biochar modification process can be mainly classified into chemical and physical activation (see Figure 6). Additionally, it is also worth mentioning that biochar engineering is gaining recent popularity as it allows for improving the catalytic efficiency and the remediation performance of biochar.

Chemical activation may be performed either before or after the pyrolysis process by blending the feedstock or biochar, respectively, with chemical agents such as acids, bases, and oxidants (Xu et al., 2021). This type of activation increases the biochar microporosity, reduces the mineral matter and also significantly increases the functional groups on the biochar surface (Gupta et al., 2022). In contrast, physical activation methods mainly include steam activation, and gas activation, such as CO₂, N₂, NH₃, O₂, air or their mixtures, or ball milling modification. All these post-pyrolysis methods may not only considerably change the surface area, pore volume and pore distribution of biochar but also affect, to a lesser extent, its surface chemical properties such as surface functional groups, hydrophobicity, and polarity (Enaime et al., 2020; Tan et al., 2017).

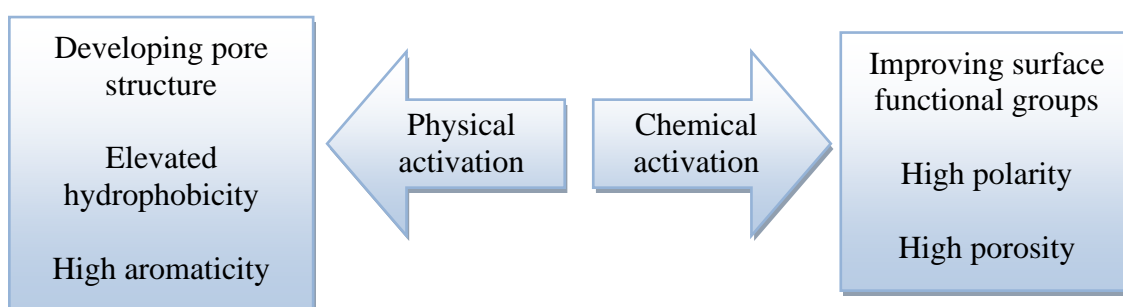


Figure 6. Main changes in biochar properties resulting from different activations (Krasucka et al., 2021).

Following this line of research, it is hypothesised that is feasible to produce a CO₂-physically modified biochar capable of effectively removing various types of pesticides from wastewater.

2. OBJECTIVES

The main objective of this work is focused on synthesizing CO₂-physically activated biochar from the biomass waste valorisation, specifically from rice husk feedstock, and testing whether it is effective as an adsorbent to remove three micropollutants with different partition coefficient n-octanol/water (clothianidin, thiacloprid and atrazine) from wastewater.

In parallel, to better understand and achieve the main goals, more specific objectives are also proposed:

- Assessing the effectiveness of the pre-treatment used to remove the silicon content of the feedstock.
- Evaluating the changes produced in biochar properties by activating it physically with carbon dioxide.
- Studying the affinity of biochar toward the three pesticides, when presented both individually and simultaneously in the aqueous solution.
- Evaluating the influence of pH on the adsorption capacity of the three pesticides on biochar and determining whether the electrostatic interactions are the main adsorption mechanism between pesticide-biochar.
- Finding a good isotherm model which can describe the adsorption process of each pesticide onto biochar.
- Studying and comparing the influence of the water matrix on the adsorption process, assessing the competition of other compounds in the wastewater matrix.

3. MATERIALS AND METHODS

3.1. CHEMICALS AND REAGENTS

3.1.1. Micropollutants

Relevant chemical information about the priority micropollutants employed in this project is gathered in Table 3. All compounds were analytical grade standards purchased from Sigma-Aldrich (Germany). These pesticides were mainly selected according to their octanol-water partition coefficient (see Table 1) as this parameter may significantly affect the adsorption process.

Table 3. Main information of the micropollutants employed in this project.

Compound	Abbreviation	Molecular Formula	Molecular Weight (g mol ⁻¹)	CAS Number
Atrazine	ATZ	C ₈ H ₁₄ ClN ₅	215.68	1912-24-9
Clothianidin	CTD	C ₆ H ₈ ClN ₅ O ₂ S	249.68	210880-92-5
Thiacloprid	TCP	C ₁₀ H ₉ ClN ₄ S	252.72	111988-49-9

3.1.2. Other chemicals

Table 4 summarizes the rest of the chemical reagents employed in this project, including information about its molecular formula, the company from was acquired and its usage.

Table 4. Summary of all the rest chemical reagents used in this project.

Name	Molecular Formula	Company	Used for
Acetonitrile	CH ₃ CN	Fisher	- HPLC analysis - Adsorption experiments
Orthophosphoric acid	H ₃ PO ₄	Panreac	- HPLC analysis - pH adjustment
Calcium chloride	CaCl ₂	Panreac	- pH _{FZC} measurement

Table 4. (continued)

Name	Molecular Formula	Company	Used for
Sulphuric acid	H ₂ SO ₄	Panreac	- pH adjustment - Buffer at pH 2
Acetic acid	CH ₃ COOH	Panreac	- Buffer at pH 4
Sodium acetate	CH ₃ COONa	Panreac	- Buffer at pH 4
Dipotassium phosphate	K ₂ HPO ₄	Panreac	- Buffer at pH 7 and pH 12
Potassium phosphate monobasic	KH ₂ PO ₄	Panreac	- Buffer at pH 7
Sodium bicarbonate	NaHCO ₃	Panreac	- Buffer at pH 10 - Buffer at pH 10
Sodium carbonate	Na ₂ CO ₃	Panreac	- Remove impurities from biomass
Sodium hydroxide	NaOH	Panreac	- pH adjustment - Buffer at pH 12
Hydrochloric acid	HCl	Panreac	- Alkalinity
Nitrogen	N ₂	Abelló Linde	- Synthesize biochar
Carbon dioxide	CO ₂	Abelló Linde	- Activate biochar

3.2. WATER MATRIX

3.2.1. Milli-Q water

The main adsorption study research presented in this work was performed with ultrapure water (UPW), produced by a Milli-Q purification system (Millipore, USA), with an average resistivity of 18.2 MΩ cm and a Total Organic Carbon (TOC) < 2 ppb.

3.2.2. Wastewater samples

The real application section of this project was performed with a secondary effluent, collected from the WWTP located at Gavà - Viladecans. Specifically, the wastewater was from the output of a line which uses an integrated fixed-film activated sludge (IFAS) system, a combination of the conventional activated sludge (CAS) and separation by ultrafiltration. The main physicochemical characteristics of this secondary effluent are listed in Table 5.

Table 5. Main physicochemical parameters of the secondary effluent employed.

Parameter	Value
pH	7.6
UV ₂₅₄ (cm ⁻¹)	0.3
TOC (mg C L ⁻¹)	25.0
NO ₃ ⁻ /NO ₂ ⁻ (mg L ⁻¹)	< 0.4
Alkalinity (mg CaCO ₃ L ⁻¹)	414.4
Total Suspended Solids (mg L ⁻¹)	38.0

3.3. BIOMASS MATERIAL

Rice husk (RH) was collected from a local agricultural region in Mocache Canton, Ecuador. The husk was firstly reduced in size by a ball mill and, subsequently, sieved to achieve the size of 250 µm. The reduced feedstock was washed with a sodium carbonate solution at constant stirring for 72 h to remove dirt and water-soluble impurities such as silicon content. The resultant material was dried at room temperature and later in an air oven at 60 °C for 24 h. Once the weight was steady, rice husk was ready to use as feedstock for biochar production.

3.4. EXPERIMENTAL DEVICES

3.4.1. Synthesis and activation of biochar

The biochar synthesis process consisted of two stages: carbonization and activation. Both the carbonization and physical activation processes of the rice husk biochar (RHB)

were carried out in a high-temperature horizontal tube furnace (stainless steel 1000 x 30 mm) KOSMON customised (see Figure 7). It was equipped with a homogeneous heated zone (100 x 30 mm) and a temperature controller with 8-stage heat treatments.



Figure 7. Experimental device to synthesize the rice husk biochar.

3.4.2. Adsorption experiments

The adsorption experiments were performed using the batch adsorption technique. The experimental setup (see Figure 8) includes a set of 100 mL graduated glass bottles as reactors for the adsorption study of each pesticide, whereas 1 L bottles were also used to test the mixture of the three micropollutants simultaneously. These different bottles were placed on an orbital shaker to mainly guarantee a correct agitation without affecting the biochar structure. The Fisherbrand™ Multi-Platform Shaker (Figure 8 – left) was mainly employed for the adsorption isotherms studies and the mix of pollutants, whereas for the rest of the experiments, the shaker used was the Cole-Parmer™ SSM1 Stuart™ Orbital Shaker (Figure 8 – right).



Figure 8. Experimental device for adsorption experiments.

3.5. ANALYSES

3.5.1. Micropollutant concentrations

The concentration of all three pesticides during adsorption experiments was quantified by High Performance Liquid Chromatography (HPLC Infinity Series, Agilent Technologies). The HPLC column used was a Teknokroma C-18 Mediterranean Sea (250 mm x 4.6 mm; 5 μ m particle size). Referent the mobile phases, acetonitrile (ACN) and ultrapure water acidified with orthophosphoric acid (at pH ~3) were used in different volumetric proportions depending on each method (see Table 6). The flow rate was set around 1 mL min⁻¹. The sample injection volume varied from 3 to 100 μ L depending mainly on the compound and the range of concentrations to be determined. All samples were injected directly after filtration through 0.45 μ m PTFE membranes.

Table 6. Method characterization for each micropollutant.

Micropollutant	% ACN	% UPW (at pH ~ 3)	Detection (nm)
CTD	50.0	50.0	268.4
TCP	50.0	50.0	242.4
ATZ	60.0	40.0	220.4

3.5.2. Wastewater analysis

Alkalinity

The alkalinity of the wastewater sample was measured through a potentiometric titration method with a SensIONTM + MM374 pH multimeter (Hach, USA). The titration was conducted with 0.1M HCl and the pH of 4.3 was fixed as the endpoint. Alkalinity is related to the ability of water for neutralizing acids.

Total Organic Carbon (TOC)

Total organic carbon content was quantified following the Standard Methods 5310B procedure (APHA, 2005). It was employed a 5055 TOC-VCSN analyser equipped jointly with an ASI-V autosampler, both from Shimadzu (Japan).

pH measurement

The pH resultant of the wastewater sample was measured with a SensION™ + MM374 multimeter, correctly calibrated every 24 hours with pH 4.00, 7.00 and 10.00 buffers.

Total Suspended Solids (TSS)

The total suspended solids correspond to the amount of tiny particulate matter that remains in suspension in water. TSS content was measured by the experimental setup shown in Figure 9. Briefly described, a 0.45 µm MF-Millipore™ Membrane Filter was weighed and placed into the filter holder of the funnel filtration membrane. With the turned-on vacuum pump, the water sample passed through this filter. Then it was placed in the oven for about 2 h and later, 1 h in the desiccator until it was at room temperature. Finally, it was weighed again and by weight difference, the total suspended solids content was calculated.



Figure 9. Assembly for total suspended solids determination.

Ultraviolet absorbance

Spectrophotometer DR6000 UV-Vis (Hach, USA) was used for measuring ultraviolet absorbance. Specifically, the ultraviolet absorbance at 254 nm (UV₂₅₄) is a characteristic parameter to give information about the level of unsaturated carbon bonds of the organic compounds (aromaticity).

3.5.3. Biochar characterization

The different characterization tests, as well as the measurement instruments employed in this section of the study, are presented further below.

pH and Electrical Conductivity (EC)

Biochar may present organics and inorganics active groups on its surface which can alter the pH of the solutions to which it is added. Therefore, the pH of both non-activated and activated biochar was measured according to Fidel et al. (2017) method. Briefly, biochars were mixed with deionized water at a 1:10 (w/v) ratio, equilibrated for 1 h and measured the pH of the solution by SensION™ + MM374 pH multimeter (Hach, USA). Employing the same equipment but with a conductivity probe, the same mixtures were equilibrated for 24 h and then measured for electrical conductivity.

Point of zero charge (pH_{PZC})

The point of zero charge is an important characteristic parameter of biochar since it provides information about its acidity/basicity and its net surface charge in solution (El-Sayed et al., 2014). The pH_{PZC} was determined by employing the pH drift method (Stephanie et al., 2021). Several 20 mL aliquots of 0.1M NaCl solutions were prepared and adjusted from pH 3 to pH 12 through 0.1M H₂SO₄ and 0.1M NaOH. Subsequently, 20 mg of activated biochar sample was added to each of these aliquots and shaken at 280 rpm for 24 h. The difference between the final and initial pH values was plotted against the pH_{initial}. The pH_{PZC} is reported as the intersection point of the curve at which $\Delta\text{pH} = 0$.

Proximate analysis

Moisture content (M_C) was quantified according to the American Society for Testing and Materials (ASTM) D2867 procedure (CEFIC, 1986). Biochar samples were weighed before and after drying in an air oven at 105 °C for 24 h. The moisture content in both biochars was calculated using Equation (4).

Ash content (A_C), which represents the not organic fraction of the moisture-free biochar, was determined by ASTM D2866 procedure (CEFIC, 1986). Crucibles with ~1.00 g of biochar samples were placed in the N 11/HR Chamber Furnace (Nabertherm, Germany) (see Figure 10) at 650 °C for 13 h to achieve a constant weight. The ash content in both non-activated and activated biochar was calculated by Equation (5).

Volatile matter (V_D) refers to content that becomes gaseous when heated above 950 °C. It was determined by International Organization for Standardization (ISO) 562-1981 procedure (CEFIC, 1986). Approximately 1.00 g of different biochar samples were also placed into the N 11/HR chamber furnace (Nabertherm, Germany) at 950 °C but only for 7 minutes. The volatile matter content of biochars was calculated by Equation (6).

$$M_C = \frac{B - F}{B - G} 100 \quad (4)$$

$$A_C = \frac{F - G}{B - G} 100 \quad (5)$$

$$V_D = \frac{100 (B - F) - M_C (B - G)}{(B - G) (100 - M_C)} 100 \quad (6)$$

Where G is the mass of the container (g), B is the mass of the container with the original sample (g) and F is the mass of the container with the dried sample (g).



Figure 10. Chamber furnace employed for measuring ash and volatile matter content.

The fixed carbon (F_C) content represents the carbon that remained in the biochar material in the pyrolysis process after the devolatilization. Fixed carbon content in both biochars was calculated from the difference between moisture, ash, and volatile matter, as shown in Equation (7):

$$F_C = 100 - \% M_C - \% A_C - \% V_D \quad (7)$$

Ultimate analysis

The ultimate analysis provides information on the elemental composition of a material (C, H, O, N, S) and can be also an indicator of both aromaticity and polarity. The CHNS and O determination both in non-activated and activated biochars was measured by duplicated through Thermo Scientific™ FlashSmart™ Elemental Analyzer, according to the ASTM D5373 method.

The specific area, pore volume and particle size distribution

The surface physical properties of non-activated and activated biochar were measured in triplicate by N₂ adsorption measurements, performed on the gas adsorption analyzer TriStar 3000 (Micromeritics, USA). Previously to measurements, biochar samples were outgassed at 40 °C overnight in a vacuum system. Nitrogen adsorption-desorption isotherms were measured at liquid nitrogen temperature (77 K) by starting at low pressure and measuring the volume adsorbed, given in cm³ STP g⁻¹ (Phuong et al., 2016). The surface area (S_{BET}) and the average pore diameter were calculated from the N₂ isotherms by the Brunauer-Emmett-Teller (BET) method and Barrett-Joyner-Halenda (BJH) method, respectively. Furthermore, the micropore volume (V_{micro}) was assessed by the t-plot method.

FESEM Analysis

Field Emission Scanning Electron Microscopy (FESEM) is a high-resolution vacuum microscopy technique that offers lofty spatial resolution images of the external morphology of materials. The surface morphology and structural characteristic of both biochar samples were assessed by using the FESEM JSM-7100-F (JEOL, Japan) (see Figure 11). The samples were previously carbon-coated to provide conductivity to the

sample and thus improve the electron signal emission. It was jointly employed a Pentaflex-INCA EDS Detector (Oxford Instruments, UK) to thus determine qualitatively the chemical composition of different selected point locations on the biochar samples.

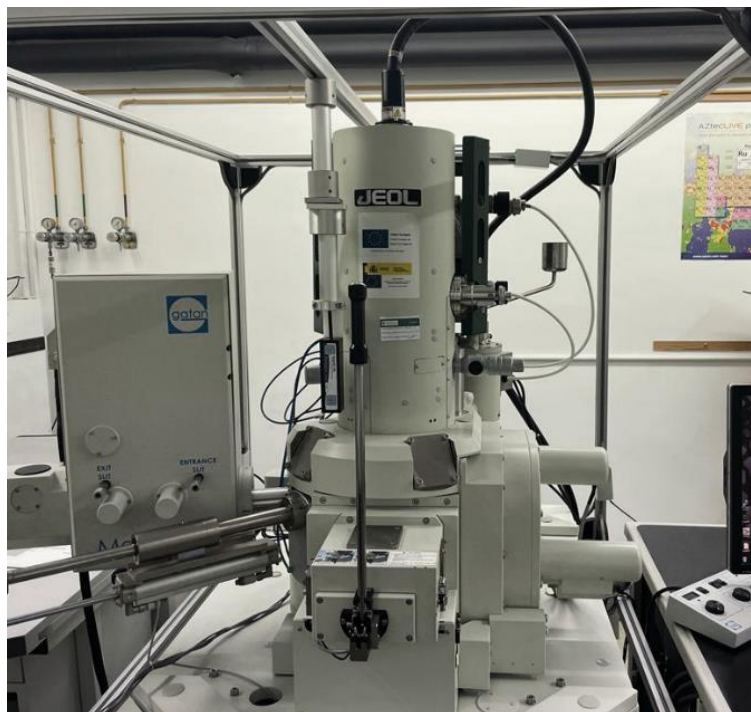


Figure 11. The FESEM JSM-7100-F used for morphology biochar samples.

Fourier Transform Infrared (FTIR) Spectroscopy

Fourier transform infrared spectra were obtained through the Spectrum Two™ FTIR spectrometer (PerkinElmer, USA). To study the different functional groups, present on the activated biochar samples surface, several scans with 4 cm^{-1} resolution were realized at wavenumbers from $450\text{ to }4000\text{ cm}^{-1}$.



Figure 12. Spectrometer employed for FTIR analysis.

3.6. EXPERIMENTAL PROCEDURE

3.6.1. Synthesis and activation biochar procedure

Concerning the carbonization step, the pre-treated feedstock was weighed, placed in boat-type ceramic crucibles, and inserted in the middle of the horizontal tube furnace. It was slowly pyrolyzed at a controlled constant flow under an N₂-H₂ (95:5) atmosphere, with a temperature ramped from ambient (~ 25 °C) to 500 °C at a heating rate of 5 °C min⁻¹. After pyrolyzing for 4 h at this target temperature, the reactor was allowed to cool down to room temperature. The resultant biochar was weighed, labelled as non-activated biochar, and stored for further activation.

Regarding the physical activation, non-activated biochar samples were previously weighed, introduced also with ceramic crucibles into the tube furnace, and kept at 800 °C for 1 h, employing carbon dioxide as the oxidizing agent and with a heating rate of 5 °C min⁻¹. The resultant biochar was weighed, labelled as activated biochar, and stored hermetically to also prevent oxidation. The conditions for both biochar carbonization and activation were chosen based mainly on a prior study, performed with old rice husk biochars, at different sizes and temperatures.

3.6.2. Adsorption experiments

Adsorption experiments for each pesticide separately were carried out in duplicate as follows:

1. Different 100 mL solutions were prepared, each one with an initial concentration of 5.00, 5.06 and 4.32 ppm for clothianidin, thiacloprid and atrazine tests, respectively. In this manner, it was ensured the same initial amount of pesticide was in each solution (2.00 μmol). (Note: in the experiments in which the pH effect was studied, 0.5 mL of different buffer solutions were previously also added, thus assuring the pH value was constant at 2, 4, 7, 10 and 12, respectively).
2. Approximately, 5.00 mg of activated biochar were added to the solutions. (Note: the biochar dosage employed in all the kinetics experiments was 50 ppm).

3. The initial pH (pre and post-adding biochar) and the initial temperature of the solutions (normally at $22\text{ }^{\circ}\text{C} \pm 1^{\circ}\text{C}$) were measured.
4. The mixtures were kept under constant stirring at 280 rpm with an orbital shaker in a time range from 0 to 74 h, in most cases providing enough time to achieve equilibrium.
5. Approximately, 1.5 mL samples were taken spread over the experiment time (more samples at shorter times and fewer at longer times) from the reactor.
6. For clothianidin experiments, each taken sample was passed directly, through a $0.45\text{ }\mu\text{m}$ PTFE filter, to the HPLC vial. In contrast, for thiacloprid and atrazine experiments, the 1.5 mL of the sample was mixed with 1.5 mL of acetonitrile in a 20 mL vial and carefully shaken. Subsequently, a 1.5 mL volume from the resultant mixture was passed through a $0.45\text{ }\mu\text{m}$ PTFE filter to the HPLC vial.
7. Finally, all samples were analysed following their respective method (see Table 6) in the HPLC.
8. Once the experiment was finalized, all the resultant pH and final temperatures were measured again.

For the isotherms adsorption experiments, 100 mL solutions containing different initial concentrations of pesticides (from 0.5 ppm to 25 ppm) were prepared. The biochar dosage employed in all these experiments was also 50 ppm. The samples were shaken at 280 rpm for 200 h at pH~7. When equilibrium was reached, 15 mL of each sample was quickly filtered into a 20 mL vial using a $0.45\text{ }\mu\text{m}$ PTFE filter. Then, 1 mL was added to HPLC vials and analysed.

The adsorption experiments of the three pesticides simultaneously at low concentrations were performed by using a 1 L solutions, both Milli-Q water and wastewater, with an initial concentration of TCP, ATZ and CTD of approximately $2.0\text{ }\mu\text{mol L}^{-1}$. A small quantity of biochar was added to the mixture. Steps 3-5 were nearly identical to those described above, with the exception that the amount of sample taken in this case was 15 mL. This quantity was rapidly filtered into a 30 mL vial using a $0.45\text{ }\mu\text{m}$ PTFE filter and then ~1 filtered mL was put into HPLC vials and analysed using a new HPLC method created specifically for these three micropollutants.

4. RESULTS AND DISCUSSION

This chapter summarizes the most relevant results obtained in this research project. The results and discussion chapter can be mainly divided into four sections. Section 4.1 includes previous studies performed with other rice husk biochars and control tests for pesticides. Section 4.2 is mainly dedicated to the characterization of the biochar produced, both non-activated and activated. Section 4.3 includes all the adsorption individual studies of the three pesticides, including pH effect and isotherms adsorption. Finally, Section 4.4 is a real application section, mainly focused on the mixing studies of the three pesticides for water and wastewater matrix.

4.1. PREVIOUS STUDIES AND CONTROL TESTS

4.1.1. Adsorption tests

The n-octanol-water partition coefficient is the ratio between the concentration of a chemical in the n-octanol phase and the water phase at a specified temperature. Therefore, this coefficient measures the differences in solubility of a chemical in these solvents and indicates its hydrophilic or hydrophobic character. If the log K_{ow} value is relatively high, approximately above one, the substance is significantly lipophilic i.e., soluble in fats and lipids solvents. Conversely, if the log K_{ow} values are below 1, the chemical is considered to be rather hydrophilic, i.e., soluble in water.

Within the MPs selected, the atrazine and thiacloprid pesticides presented a log K_{ow} value higher than one, namely 2.61 and 1.26, respectively. For this reason, it was assessed the adsorption effect of both pesticides, and just in case also clothianidin (log $K_{ow} = 0.7$), on the experimental material to be used (HPLC filters, syringes, and pipette tips) since these might be adsorbed on them and cause a markedly experimental error.

Adsorption from syringes and pipette tips

None of the three proposed contaminants (CTD, TCP and ATZ) was adsorbed by the syringes or the pipette tips employed in the experiments. It could be mainly because the contact time was minimal.

Adsorption from HPLC filters

At first, the adsorption was studied with a nylon 0.45 μm filter for CTD, the pesticide with the lowest n-octanol-water partition coefficient. In all conditions tested, the results showed an adsorption value lower than 2 %. For TCP, whose log K_{ow} value was higher, tests were also repeated in triplicate, and the average adsorption for small quantities at higher concentrations (5 ppm) was about 5 %, whereas, at lower concentrations (0.5 ppm), the adsorption increased to around 11 %. Therefore, it was decided to work by dilution (50:50) with acetonitrile before filtering, and avoid thus adsorption of TCP on the filter. As ATZ presented the highest log K_{ow} , tests were directly carried out with this dilution technique. The resultant adsorption for both pesticides (TCP and ATZ) with this method was less than 5 % when passing through filters for all concentrations tested.

4.1.2. Previous biochar studies

Some preliminary experiments with CTD were conducted to find the most optimal synthesis conditions leading to the production of a rice husk biochar with remarkable properties. We were given 8 rice husk biochar samples, which had already been synthesised and physically activated by another group. The variables studied were biomass size and the pyrolysis and activation temperature (see Table 7). (Note: both the pyrolysis and activation time for all biochar samples were 4h and 1h, respectively, so it was not a variable studied in this project).

Table 7. Main variables of rice husk biochar samples to study in the preliminary experiments.

Sample	Biomass size	Pyrolysis temperature	Activation temperature
1	100 μm	500 $^{\circ}\text{C}$	600 $^{\circ}\text{C}$
2			800 $^{\circ}\text{C}$
3		700 $^{\circ}\text{C}$	600 $^{\circ}\text{C}$
4			800 $^{\circ}\text{C}$
5	250 μm	500 $^{\circ}\text{C}$	600 $^{\circ}\text{C}$
6			800 $^{\circ}\text{C}$
7		700 $^{\circ}\text{C}$	600 $^{\circ}\text{C}$
8			800 $^{\circ}\text{C}$

Figure 13 shows the comparison between the different activation temperatures studied, i.e., 600 °C and 800 °C, both at 1 h of constant temperature. It was observed that biochar activated at 800 °C achieved around 100 % CTD adsorption in 96 h in all cases, independently of the biomass size and the pyrolytic temperature. However, for biochars activated at 600 °C, at the same time, only 40.29 % was adsorbed in the best case. The resultant adsorption profiles of these preliminary experiments are gathered in Annex 1.

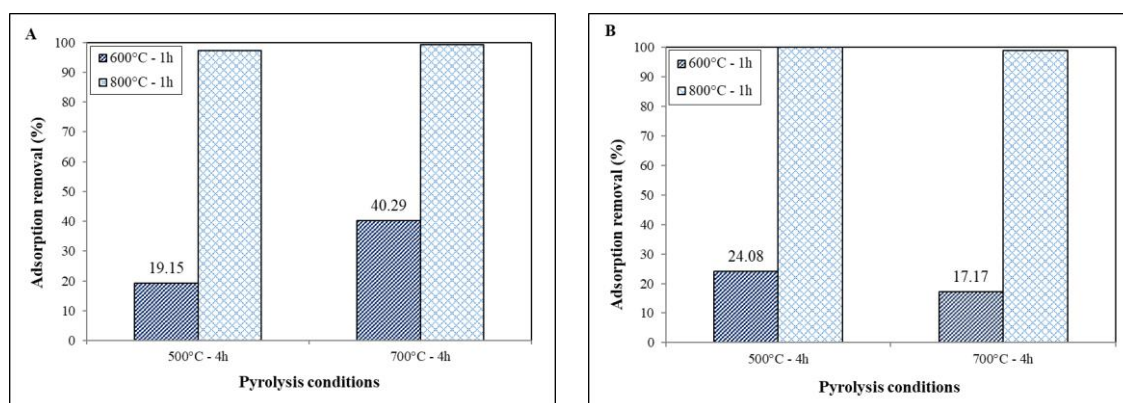


Figure 13. CTD adsorption removal (%) at different activation temperatures with biochars from (A) 100µm and (B) 250µm biomass sizes. [CTD]_o = 0.1 mg L⁻¹; [BC] = 500 mg L⁻¹; T = 22.3 °C; Time = 96 h.

Table 8 shows the carbon and silicon content of the different biochars activated at 800 °C, obtained from two different biomass sizes (100 and 250 µm). It was noticed that, in this case, biochars produced from smaller biomass had a higher silicon content and a lower carbon percentage compared to those biochars from 250 µm rice husk size. According to Ahiduzzaman & Islam (2016), rice husk biochars with a high amount of silica may inhibit biochar porousness.

Table 8. Carbon and silicon content in the 800 °C activated biochars from different biomass sizes.

Sample	Biomass size	Pyrolysis temperature (°C)	% C	% Si
2	100 µm	500	31.6	52.0
4		700	35.0	30.7
6	250 µm	500	48.0	26.3
8		700	70.2	17.1

Regarding the pyrolytic temperature, results were in line with Singh Karam et al. (2021), which indicated that performing two thermal processes (carbonisation and activation) at such elevated temperatures might destroy the typical morphological pattern of rice husk biochars.

Having explored the different variables to examine in these preliminary studies, and due to the briefly aforementioned reasons, it was opted to synthesise our biochar from 250 μm pre-treated rice husk, using 500 °C and 800 °C as the pyrolysis and activation temperatures, respectively, as it is detailed in Section 3.6.1.

4.2. BIOCHAR CHARACTERIZATION

The results obtained from the different characterisation tests carried out with the biochar synthesised in the current work are detailed below.

4.2.1. Basic properties

The electrical conductivity, pH, and yield resultant of both activated and non-activated biochar are gathered in Table 9.

Table 9. Yield, pH, and EC data for non-activated and activated rice husk biochar.

Biochar	Yield (%)	pH	EC (mS cm ⁻¹)
Non-activated	40.09	10.73	5.82
Activated	26.95	11.06	8.01

The **biochar yield** corresponded to the amount of biochar produced relative to the total amount of initial feedstock. The experimental outcomes indicated that non-activated biochar achieved a 40.09 % yield in the carbonisation step, which was within the typical expected range, as was indicated in Table 2. In contrast, considering simultaneously two-step pyrolysis, i.e., carbonisation and activation steps, the biochar achieved only the 26.95 %. This 13.14 % reduction in yield during the activation stage could be mainly attributed to the presence of a secondary pyrolysis reaction and, the subsequent loss of

volatile matter by thermal cracking at such high temperatures (Sahoo & Remya, 2020; Singh Karam et al., 2021).

Regarding the **pH**, lower pyrolysis temperatures result in acidic biochars, whereas higher temperatures produce biochars with more alkaline properties (Jung & Kim, 2014). According to Shi et al. (2019), the resultant biochar pH is a balance between its acidic functional groups, such as -COOH, and its alkaline minerals, and both can affect strongly in the adsorbent properties. The resultant pH values of our biochar were considerably alkaline, 10.73 and 11.06 for non-activated and activated, respectively. Therefore, it was not expected to find many acidic functional groups in biochar surfaces when performing the infrared spectra. Furthermore, as also indicated by Singh Karam et al. (2021), the high pH level of rice husk biochar could be mainly attributed to its ash content, which might contain alkaline carbonates, alkali earth metals or organic anions.

The **electrical conductivity** of biochar, which is related to the quantity and nature of salts dissolved in solution, increased from 5.82 to 8.01 mS cm⁻¹ through the physical activation with CO₂. According to Singh et al. (2017), this enhancement could be mainly attributed to the high concentration of ash caused by the loss of volatile matter during the activation step. In addition, as stated by Park et al. (2021), it might also be due to the crystallization of carbon elements, after the cellulose was thermally decomposed.

4.2.2. Proximate analysis

The proximate analysis was performed to assess the moisture, volatile matter, ash, and fixed carbon content of both biochars. Results from this analysis are listed in Table 10.

Table 10. Moisture, volatile matter, ash, and carbon fixed content of non-activated and activated RHB.

Biochar	Moisture (%)	Volatile matter (%)	Ash (%)	Carbon fixed (%)
Non-activated	0.64	59.32	36.28	3.76
Activated	1.57	45.89	43.21	9.32

An increment in **moisture** content from non-activated to activated biochar was observed since it increased from 0.64 % to 1.57 %. Although both resultant percentages were relatively low, this behaviour was contrary to what first was expected. According to Nidheesh et al. (2021), the moisture content decreases with an increase in the pyrolysis temperature, due basically to the loss of water molecules present in the feedstock. Therefore, when activated at 800 °C, it was expected to find a lower moisture content. However, this result could be owing to the hygroscopic nature of the resulting biochar. It might adsorb water from the air during the different cooling, weighing, or packaging processes, as also suggested by Zulkania et al. (2018).

Regarding the **volatile matter** content, namely the labile biochar fraction, it decreased from 59.32 % to 45.89 % during the physical activation process. The results followed the trend proposed by Jindo et al. (2014). Depending on the feedstock type, biochars subjected to lower pyrolysis temperatures contain a higher volatile matter content and, as increasing temperature, this volatile matter percentage gradually decreases. The 13 % volatile matter decrease, obtained during the activation stage, roughly coincided also with the aforementioned 13 % reduction in yield. Therefore, there could be a relation between these two parameters, as supported by C. Wang (2021).

The **ash** content of biochar increased also during the activation stage, specifically from 36.28 % to 43.21 %, due mainly to the increment in pyrolytic temperature. This high percentage in both biochars can be also attributed to the large ash content presented in rice husk feedstock, typically around 20 % (Jongpradist et al., 2018). Moreover, the high percentage of silica and other minerals contained in the feedstock could lead to also obtaining a high ash content, as stated by Nurul Farhana et al. (2018). However, Asadi et al. (2021) and Singh Karam et al. (2021) collected information from several studies in which ash content also was studied in biochars from rice husk feedstock, and the values ranged from 27.5 % to ~ 65 %. Therefore, the outcomes seemed to indicate that our biochars were within the expected range.

The **fixed carbon** content, related to the recalcitrant biochar fraction, varied slightly at the activation step. For non-activated biochar, it was only 3.76 %, whereas for activated increased to 9.32 %. These two poor values of fixed carbon are mainly due to the high ash content in biochars since ash particles can hinder the formation of aromatic

structures, which contribute greatly to the fixed carbon content, as explained by Choudhary et al. (2019).

Although these results were within the typical range expected when compared to other biochar studies, it could be thought that the pre-treatment employed to remove the silicon content from the rice husk raw material was not entirely effective.

4.2.3. Surface area, porosity, and physical structure

As shown in Table 11, pyrolysis carried out with N₂ at 500 °C did not lead to substantial development of the pore structure of biochar (see Figure 14), since the resultant BET surface area obtained from the carbonisation step was only 1.22 m² g⁻¹, whereas the pore volume and average pore size were 4.48·10⁻⁴ cm³ g⁻¹ and 65.78 nm, respectively.

Table 11. Surface area, pore volume and pore size results for non-activated and activated biochar.

Biochar	S _{BET} (m ² g ⁻¹)	Pore volume (cm ³ g ⁻¹)	Average pore size (nm)
Non-activated	1.22	4.48·10 ⁻⁴	65.78
Activated	379.95	0.123	5.56

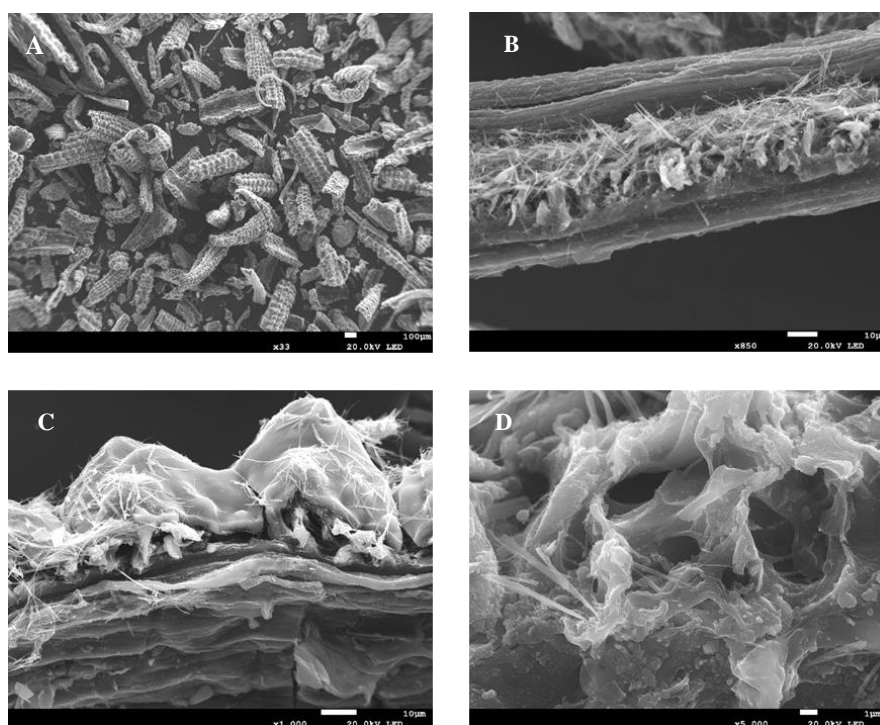


Figure 14. FESEM images of non-activated rice husk biochar (500°C-4h) at (A) x33; (B) x850; (C) x1,000 and (D) x5,000 magnifications.

Compared to pristine biochar, CO₂ physically-activated biochar was characterised by a more developed pore structure (see Figure 15). The specific surface area and pore volume resulting from the activation stage increased considerably to 379.95 m² g⁻¹ and 0.123 cm³ g⁻¹, respectively, whereas the pore size decreased to 5.56 nm.

This great variation in pore properties can be attributed also to the high temperature applied during the activation process. Pore-blocking substances (see Figure 14B), such as volatile matter or ash, were partially driven off at 800 °C, which led to an increase in the available surface area of biochar (see Figure 15B), as argued by Tomczyk et al. (2020). However, according to Nidheesh et al. (2021), part of these blocking filaments could also be inorganic crystals, such as sodium carbonate or silica crystals, and could remain engrained.

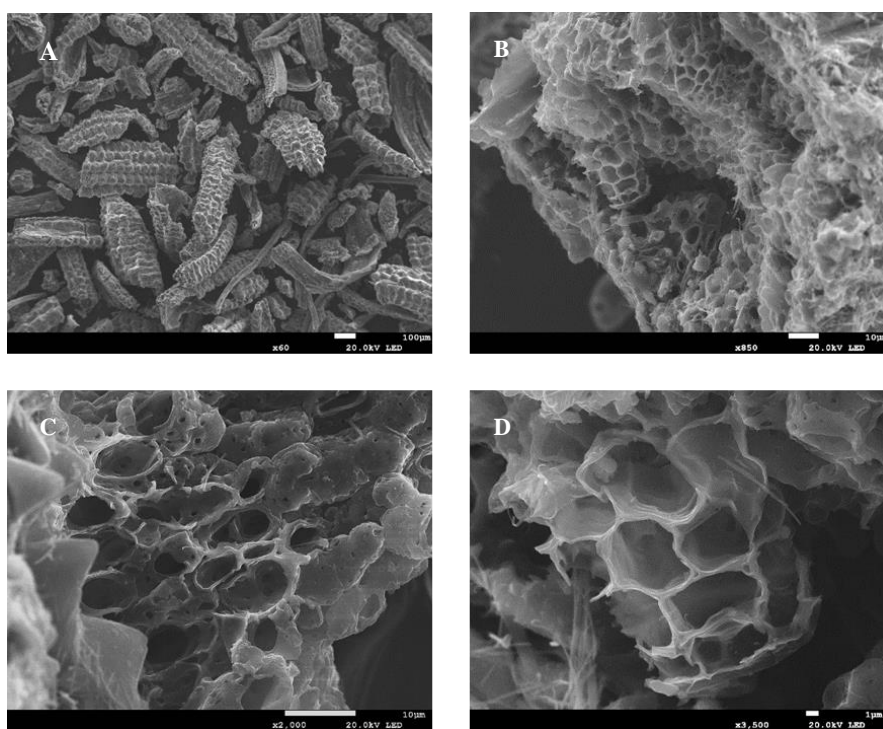


Figure 15. FESEM images of CO₂ physically-activated rice husk biochar (800°C-1h) at (A) x60; (B) x850; (C) x2,000 and (D) x3,500 magnifications.

Following the International Union of Pure and Applied Chemistry (IUPAC), biochar porosity can be mainly classified into macropores (>50 nm), mesopores (2 - 50 nm) and micropores (<2 nm) (Porada et al., 2013). At such a high activation temperature, the few macropores of non-activated biochar and the walls between all the adjacent pores might have been destroyed, thus causing more mesopores and the enlargement of specific

surface area, as suggested by Claoston et al. (2014). The average pore size in different studies of biochars ranged from 2 to 8 nm, so our biochar fell into the small mesoporous regime. In addition, as reported by Yavari et al. (2017), a rice husk biochar activated at the same conditions (800 °C for 1 h with CO₂) led to a similar S_{BET} of 334 m² g⁻¹.

In terms of surface morphology, it was mostly observed that both biochars presented a tubular structure pattern (see Figures 14A and 15A). However, the enlarged images showed morphological surface changes on the biochar upon the activation process. It changed practically from a mostly blocked porous structure with an irregular shape in non-activated biochar (see Figure 14C) to a well-developed porous, honeycomb-like structure in activated biochar (see Figures 15-B to D).

Although a compositional analysis was not technically performed for quantifying the silicon content presented in the biochar, it was possible to qualitatively verify, by EDS detector, the large amount of Si in biochar (see Figure 16). It could be confirmed the high percentage of silicon compared to other elements, and thus led to the conclusion that the pre-treatment employed to remove silica had not been entirely effective. (Note: Au peaks appeared because the coating was performed with gold in this case).

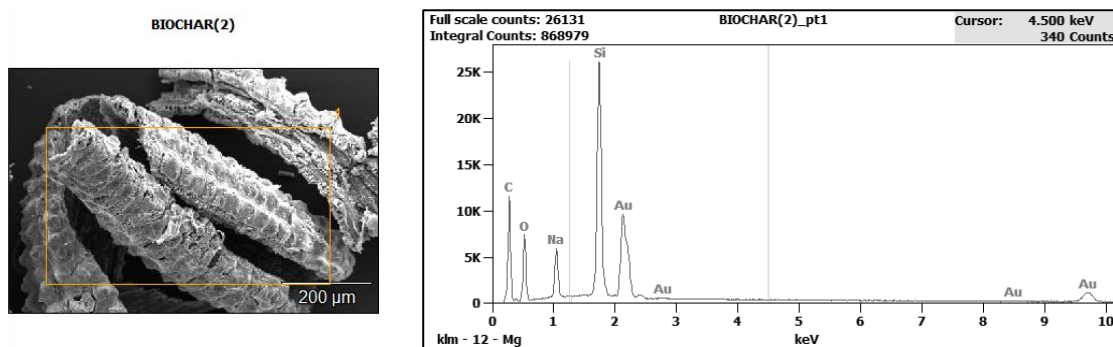


Figure 16. EDS graph of rice husk biochar.

4.2.4. Ultimate analysis

The analysis of the elemental composition of both biochars (see Table 12) indicated that during the CO₂-physically activation process, all the elemental contents were reduced, except sulphur, which slightly appeared.

Table 12. Ultimate analysis of non-activated and activated rice husk biochar.

Biochar	% C	% H	% O	% N	% S
Non-activated	56.31	1.76	7.48	0.40	0.00
Activated	37.83	0.00	5.18	0.27	0.08

As expected, the **hydrogen** and **oxygen** content decreased mainly due to the increase in the activation temperature, since occurred dehydration, decarboxylation, deacetylation, and deoxygenation reactions (Binnal et al., 2022). Furthermore, the low **nitrogen** content was within the typical range compared to other studies and it was mainly due to the loss of ammonia and oxides by carbonization process (Singh Karam et al., 2021).

The **carbon** content was considerably reduced during the CO₂ physical activation process, specifically from 56.31 % to 37.83 %. According to Jung & Kim (2014), this decrease could be mainly justified by the Boudouard reaction ($\text{CO}_2 + \text{C} \leftrightarrow 2\text{CO}$). At such high temperatures, above 800 °C, the carbon atoms of biochar are mainly removed by CO₂, resulting in increased combustion. This could also complement the explanation of the morphology transformation (from macropores into mesopores) or the high amount of ash produced during the activation process.

The **H/C atomic ratio** for non-activated biochar was approximately 0.03, whereas, for the CO₂-physically activated biochar, it decreased to 0.00. This outcome indicated that the carbonization of biochar was complete upon activation and the resultant biochar presented long-term environmental stability. Conversely, the **O/C atomic ratio** for non-activated and activated biochars were 0.14 and 0.13, respectively. As this ratio was below 0.2, it could indicate that both biochars presented low polarity. These both low ratio values were in line with the results suggested by Conte et al. (2021).

4.2.5. FTIR spectra

The **FTIR spectra** of the RHB activated with CO₂ for 1 h at 800 °C were provided in Figure 17. The non-appearance peaks in the wavenumber regions between 3600-3100 cm⁻¹ corresponded to an absence of hydroxyl groups, thus corroborating the low polarity of biochar. The tiny peaks observed at 2987 and 2883 cm⁻¹ could be related to the C-H

stretching vibration, but the lack of H content made us doubt it, whereas the weak vibration shown in the 2000-2400 cm^{-1} region corresponded to equipment noise. According to Morales et al. (2021), the peak shown in the band 1430 cm^{-1} could be related to C-O stretching. However, Jindo et al. (2014) proposed C=C stretching for the same band. The intense band at 1047 cm^{-1} can be assigned to stretching vibrations of the Si-O bond (Morcali et al., 2013). The bands found around 787 cm^{-1} and 618 cm^{-1} could be attributed to the bending and stretching vibration of the Si-O-Si group, respectively (Saha et al., 2014). These outcomes agreed with the aforementioned high silicon content and showed low surface functional groups.

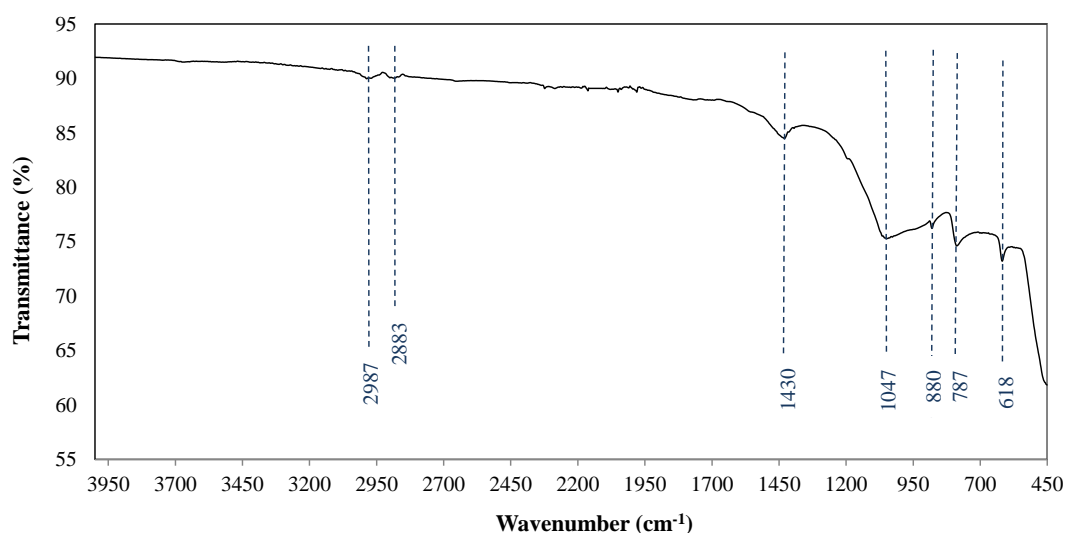


Figure 17. FTIR spectra of rice husk biochar activated with CO_2 at 800 °C for 1 h.

4.2.6. Point of zero charge

Figure 18 presents the resultant pH_{PZC} value for the CO_2 -activated rice husk biochar. By interpreting this profile, it could be noticed that the resultant pH_{PZC} value was 10.23. Therefore, when operating at pH conditions below this point, the biochar surface was positively charged. In contrast, the residual charge on the biochar surface, at pH values higher than 10.23, was negative as indicated by do Nascimento et al. (2022). Further explanation will be presented in the following section about the adsorption mechanism of the pesticides into the surface biochar.

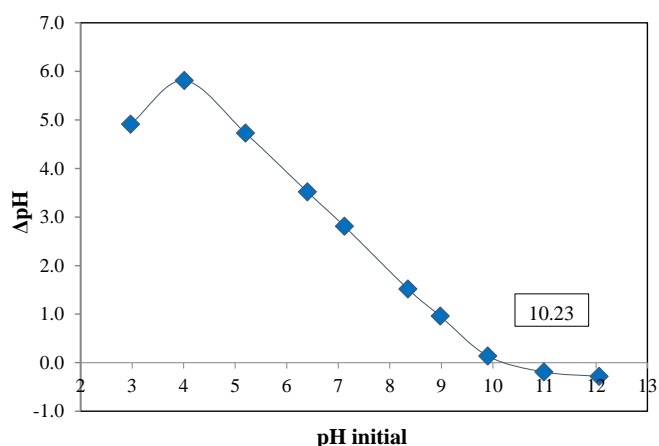


Figure 18. Experimental determination for pH_{PZC} value for activated RHB.

Completed the characterization of both non-activated and activated biochar, it could be concluded that the method used to remove the Si content from rice husk was not effective and the activated biochar showed better porosity characteristics compared to the non-activated. Therefore, it was decided to perform the adsorption studies using the CO_2 -physically activated biochar, hereafter referred to as biochar, and check whether it was able, despite its characteristics, to remove the pesticides from aqueous solutions.

4.3. ADSORPTION STUDIES

4.3.1. Adsorption at non-constant pH value

Table 13 summarises the adsorption experiments performed for each pesticide separately without maintaining the pH value constant. It mainly includes the pesticide studied, with its initial and final amount, the adsorption achieved per gram of adsorbent, as well as the initial and final pH values.

Table 13. Summary of the experimental results for the adsorption of each pesticide separately with $[\text{BC}]_0 = 50 \text{ mg L}^{-1}$.

MP	pH_0	pH_F	MP initial amount (μmol)	MP final amount (μmol)	Adsorption ($\mu\text{mol g}^{-1} \text{ BC}$)
CTD	8.58	7.48	1.95	0.99	178.61
TCP	8.95	7.45	1.99	1.25	139.78
ATZ	8.81	7.35	1.95	1.46	94.05

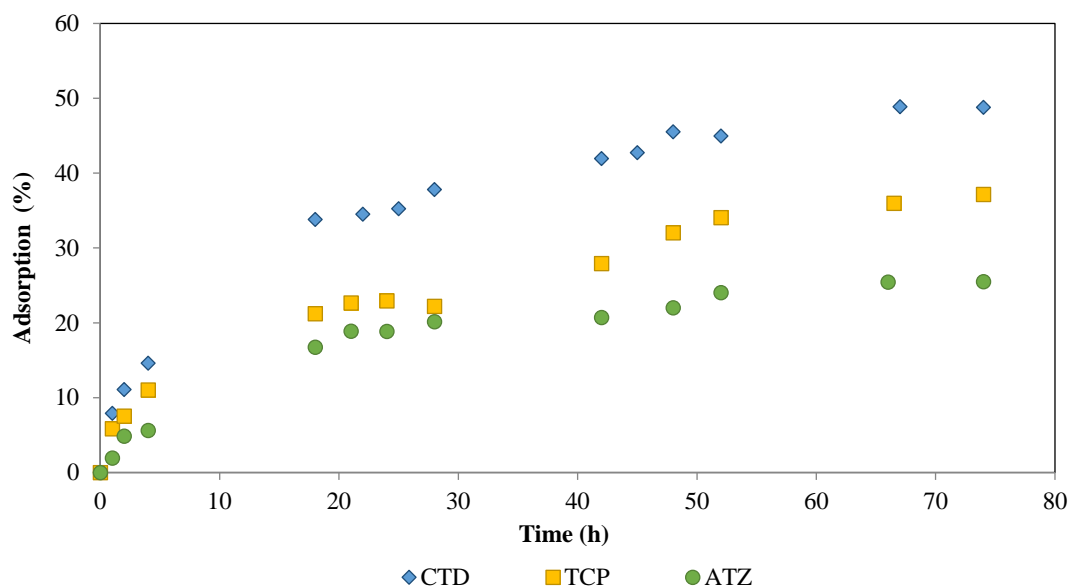


Figure 19. Adsorption profiles of CTD, TCP and ATZ individually on rice husk biochar. $[MP]_0 = 20 \mu\text{mol L}^{-1}$; $[BC]_0 = 50 \text{ mg L}^{-1}$; $T = 22 \text{ }^\circ\text{C}$.

As shown in Figure 19, under the same initial conditions, each pesticide was adsorbed differently on the biochar surface. Regarding the clothianidin, the most hydrophilic pesticide used, seemed to have the highest affinity for biochar since, for each gram of this adsorbent, $178.61 \mu\text{mol}$ were removed from the aqueous phase (see Table 13). This corresponded to $\sim 48.78 \%$ of adsorption. In contrast, at the same time and conditions, the adsorption achieved for TCP and ATZ was 139.78 and $94.05 \mu\text{mol g}^{-1}$, respectively, which corresponded approximately to 37.15% and 25.52% .

This trend seems to indicate that biochar had a higher attraction for more hydrophilic compounds than for hydrophobic ones. Initially, the opposite effect was expected since according to X. Wang et al. (2020), the removal of hydrogen- and oxygen-containing functional groups at elevated temperatures (in our case, during the activation stage) could lead to more hydrophobic biochars. However, the inorganic matter, such as silica, contained in the ash particles was probably more hydrophilic than the carbon skeleton in biochar. Therefore, the few polar silicon-containing functional groups of ash particles could have a great impact and favoured biochar affinity toward more hydrophilic compounds, such as clothianidin (Kozyatnyk et al., 2021).

It is important also to mention that the pH values increased from approximately $5.6 - 5.8$ to $8.58 - 8.95$ when biochar was added to the solution, mainly due to the high pH value

of the biochar itself, which was 11.06. After completing the experiments, the final pH values decreased to 7.35 - 7.48, thus showing the low buffering capacity of biochar, as also claimed by Meirkhanuly et al. (2019).

4.3.2. Adsorption mechanism

To better elucidate the adsorption mechanisms, such as electrostatic interactions, of the three pesticides onto biochar, the correlations between the pKa value of the adsorbates, the medium pH, and the biochar surface charges were assessed in this part. Different experiments were carried out for each pesticide at different pH levels (2, 4, 7, 10 and 12). The outcomes obtained are shown in Figure 20.

Clothianidin, being a basic specie with a pKa-value of 11.09, was deduced to be in its cationic form at $\text{pH} < \text{pKa}$, whereas its neutral form was predominant for $\text{pH} > \text{pKa}$. Relating this to the surface residual charge of biochar ($\text{pH}_{\text{PZC}} = 10.23$), originally, it was expected that, for pH values between 2-10, electrostatic repulsions would exist between the amine-protonated ($-\text{NH}_2^+$) species of CTD and the biochar surface, also positively charged. For pH values ranging from 10.23 to 11.09, an attraction was expected, as the CTD was positively charged while the surface of biochar presented a negative residual charge. Finally, at pH values above 11.09, the repulsive forces would be lower as the CTD was in its neutral form while the surface of biochar was still negatively charged.

As can be observed in the results from Figure 20, it is true that at pH 12, i.e., $\text{pH} > \text{pKa}$, the highest adsorption was achieved (50.17 %), corresponding to $171.89 \mu\text{mol g}^{-1}$. In contrast, the minimum adsorption was at pH 4 ($\text{pH} < \text{pKa}$), which corresponded to the most positively charged state of biochar, as can be seen in Figure 18, thus existing more repulsions. However, for the other pH levels, there was also no such considerable variation, as the adsorption values achieved ranged from 37.81 % to 44.67 %. Therefore, it could be considered that electrostatic interactions did not exert an important effect on the clothianidin adsorption mechanism with this type of biochar. Other processes such as the π - π electron donor-acceptor interactions or hydrogen bonds may exert a more important role. These findings were further supported by P. Zhang, Sun, et al. (2018).

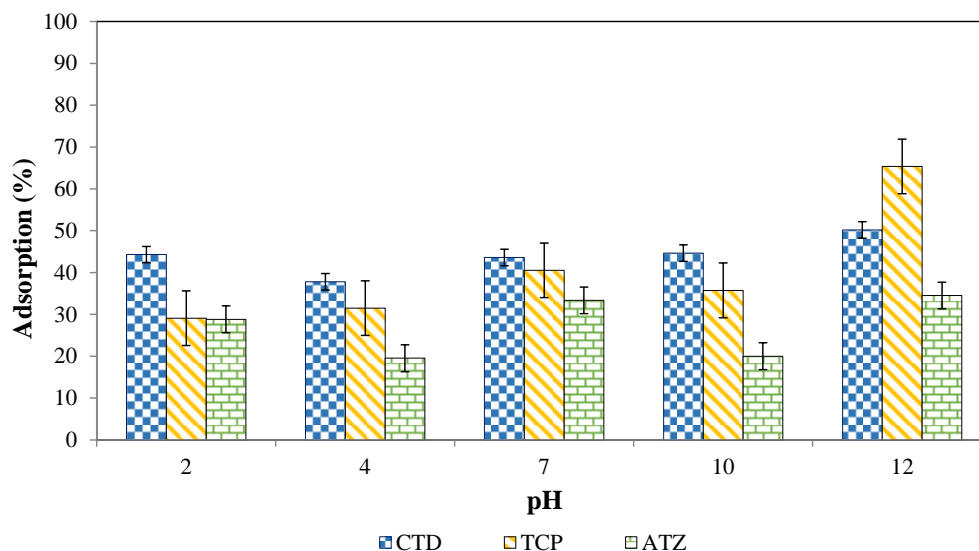


Figure 20. Adsorption percentage achieved after 74 h for CTD, TCP and ATZ at different pH values. $[MP]_0 = 20 \mu\text{mol L}^{-1}$; $[BC] = 50 \text{ mg L}^{-1}$; $T = 22 \text{ }^\circ\text{C}$

In the case of thiacloprid, it resulted more complex as no pK_a value was observed, so it was not in its ionised form, but different findings were obtained when the pH effect was assessed. At more acidic pH conditions, namely at pH 2, about $109.92 \mu\text{mol g}^{-1}$ could be removed, which corresponded to 29.09 % of adsorption. In contrast, at more basic values, such as pH 12, more than twice as much adsorption was achieved, namely 65.37 %, which was $225.29 \mu\text{mol g}^{-1}$. Excluding electrostatic interactions, the H-bonding or the π - π EDA interactions could probably be the main mechanism responsible for the TCP adsorption on biochar, as indicated by Kah et al. (2017). Therefore, it was possible to indicate that thiacloprid adsorption on this biochar was enhanced under high pH values (close to 12), but further depth studies would be required.

Atrazine, as aforementioned in Section 1.4.2., is also a basic specie presenting a pK_a value of 1.7. According to a speciation diagram constructed by do Nascimento et al. (2022), the nitrogen contained in the triazine groups can be highly protonated (NH^+) at pH values below 4. Therefore, electrostatic repulsion should occur between the biochar surface, with a positive residual charge, and these protonated ATZ species. In contrast, for pH values within the range from 6 to 12, the predominant species were in their neutral form, so the repulsion force should be gradually lower at increasing pH. However, as can be seen from Figure 20, this trend was not followed in our case, as the resultant adsorption percentage was oscillating at different pH values. Specifically, for

pH 4 and 10, only about 20 % adsorption was obtained, whereas, at pH 2, 7 and 10, between ~29-34 % adsorption of ATZ on biochar was achieved. After viewing the results obtained up to this point of the study, it was possible to conclude that electrostatic interactions were not the main adsorption mechanism of ATZ on biochar. According to Kah et al. (2017) and Xiao & Pignatello (2015), pH was expected to have little influence on ATZ adsorption and the uncharged atrazine mainly undergoes the π - π EDA interactions, respectively.

Furthermore, it could be also mentioned that for all pH values (see Figure 20), except for pH 12 which would require further research, the same trend was observed as in the section 4.3.1, since the most hydrophilic compounds (clothianidin) achieved higher adsorptions on the surface of biochar compared to hydrophobic ones (atrazine).

4.3.3. Adsorption isotherms

The equilibrium adsorption data of CTD, TCP and ATZ on biochar was assessed by applying Langmuir and Freundlich models, as previously explained in Section 1.5.3, and the results of their linear regressions were used to find out the fit model. The estimated isotherms parameters of both adsorption models, as well as the regression coefficients (R^2), for the three pesticides, were gathered in Table 14.

Table 14. Isotherms parameters for the adsorption of CTD, TCP and ATZ on biochar at pH 7 and 23 °C.

MP	Langmuir			Freundlich		
	K_L ($10^{-3} \text{ L } \mu\text{mol}^{-1}$)	Q_{max} ($\mu\text{mol g}^{-1}$)	R^2	K_F ($\mu\text{mol g}^{-1}/(\mu\text{mol L}^{-1})^n$)	n	R^2
CTD	4.79	4078	0.999	19.87	0.970	0.989
TCP	4.90	4068	0.998	19.99	0.978	0.995
ATZ	*n.a.	n.a.	n.a.	18.95	1.003	0.999

* n.a.: non-available

As indicated in Table 14, the experimental equilibrium results obtained for atrazine could not be linearly fitted to the Langmuir model, since the resulting estimated parameters were negative values, and therefore had no physical significance. This result might be expected, since as shown in Figure 21, the isotherm profile for atrazine did not

exhibit the classical L-curve (see Figure 5b) with a strict plateau, unlike the TCP and CTD profiles. This type of curve is mainly related to the Langmuir model and is characteristic of dilute solutions in the adsorption systems (do Nascimento et al., 2022). However, to confirm this trend, it would have been necessary to test with a higher initial concentration of atrazine, but its maximum solubility in water was close.

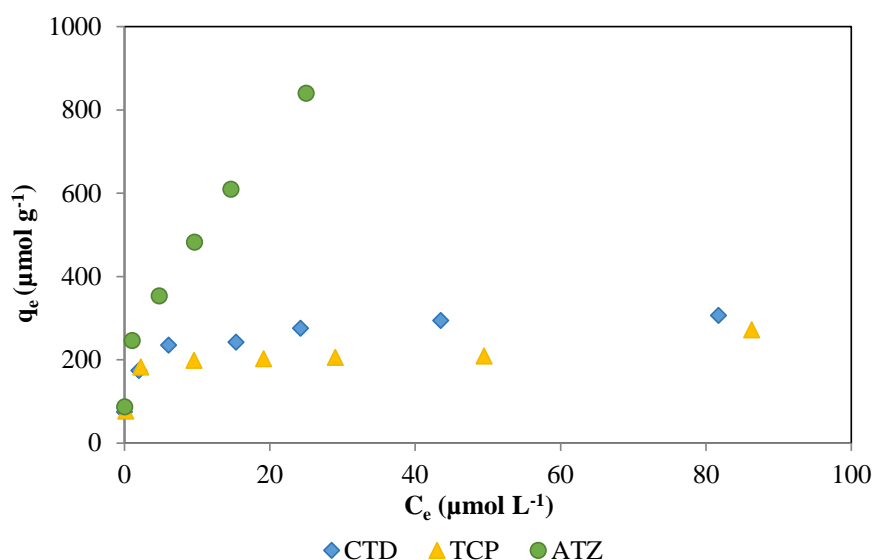


Figure 21. Experimental equilibrium data for CTD, TCP and ATZ adsorption on BC. (pH 7 and T=23 °C).

Although both models showed a high correlation coefficient ($R^2 \sim 0.99$), the two neonicotinoids data fitted better with the Langmuir model than the Freundlich one. Interestingly, both pesticides presented similar results (see Figure 22A), since the maximum adsorption capacity for CTD was $4078 \mu\text{mol g}^{-1}$, whereas for TCP was nearly $4068 \mu\text{mol g}^{-1}$. It suggested that both were adsorbed on the biochar surface as monolayers, namely, each neonicotinoid molecule occupied one active site with no competition among them, since all had the same energy.

Comparing the Langmuir constant, both outcomes also exhibited similar behaviour, as the adsorption activation energy for thiacloprid and clothianidin was $4.90 \cdot 10^{-3}$ and $4.79 \cdot 10^{-3} \text{ L } \mu\text{mol}^{-1}$, respectively. However, it might appear that thiacloprid had a slightly more affinity toward this biochar than clothianidin. Furthermore, in this case, there did not seem to be a direct relationship between the log K_{ow} coefficient of pesticides and the adsorptive capacity of biochar.

To determine the feasibility of the reactions, namely whether the adsorption system was favourable or not, the dimensionless separation factor was calculated for both TCP and CTD (as explained in section 1.5.2). The resultant values of R_L were found in the range of 0.98 – 0.62 for TCP, whereas for CTD ranged from 0.98 – 0.60. In both cases below 1, thus indicating that the adsorption of these two pesticides on biochar was favourable (Depci, 2012).

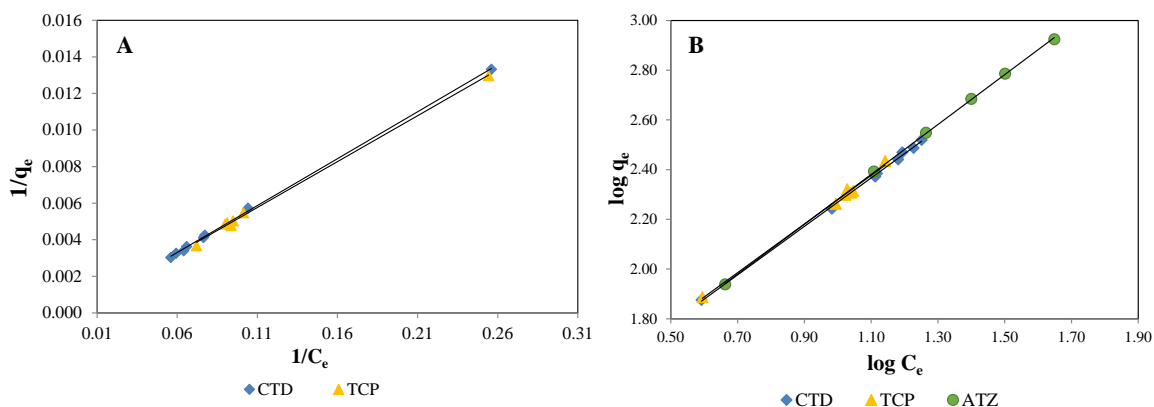


Figure 22. The linear plots of CTD, TCP and ATZ adsorption isotherms of (A) Langmuir and (B) Freundlich models on biochar. (At pH = 7 and T = 23 °C).

Regarding the atrazine adsorption on biochar, its equilibrium data were fitted to the linearized form of the Freundlich model (see Figure 22B). Due to its high coefficient of determination, it was evidenced that the Freundlich isotherm explained the adsorption phenomenon reasonably well.

The resulting Freundlich coefficient value, mainly related to the adsorption capacity, was around 18.95 ($\mu\text{mol g}^{-1}/(\mu\text{mol L}^{-1})^n$). On the other hand, the adsorption intensity or surface heterogeneity value (the n parameter), was about 1, suggesting linear adsorption for atrazine. In other words, the atrazine adsorption was approximately constant at all tested concentrations (H. N. Tran et al., 2017).

As a result, the outcomes might suggest that the atrazine-biochar system was a multilayer adsorption process with a distribution of surface energy (dos Santos et al., 2019). However, as the Freundlich model is empirical, it should be noted that the physical interpretation of the constants is not entirely reliable.

4.4. APPLICATION WITH REAL WASTEWATER

Most wastewaters contain a variety of compounds which might mutually enhance, interfere, or act independently in the adsorption process. In order to further explore the applicability of this biochar to real water environments, three final experiments (see Table 15) were conducted with all three pesticides simultaneously. Specifically, it was studied the adsorption capacity of the biochar at different initial concentrations of these pesticides (high and low-typical range) for different water matrices (milli-Q and wastewater).

Table 15. Summary of the main experiments, and their initial conditions, in the real application section.

(Note: MP₀ refers to CTD, TCP and ATZ)

Exp	Water matrix	MP₀ (μmol)	BC₀ (mg L⁻¹)	pH
1	Milli-Q	20.00	50.00	Adjusted to 7.0
2	Milli-Q	2.00	50.00	Adjusted to 7.0
3	Wastewater	2.00	50.00	~ 7.6

As can be observed from Table 15, no experiment at high pesticide concentrations was performed with wastewater matrix, since micropollutants in wastewater are normally at trace levels, therefore it would not be realistic. Furthermore, the pH of the milli-Q water matrix was also adjusted to pH 7, to approximate thus the real value of the wastewater.

First, we sought to test the identical conditions that had been applied for the individual experiments, namely high initial pesticide concentrations and a milli-Q water matrix. The goal was to determine for which of the three pesticides, biochar had the highest affinity. As shown in Figure 23, when all pesticides were mixed, biochar clearly showed a higher preference for thiacloprid, since each gram of biochar managed to remove from the aqueous solution approximately 82.62 μmol of TCP at 74h. However, at the same time, merely 28.26 and 22.84 μmol g⁻¹ of CTD and ATZ, respectively, were adsorbed. These findings were in line with the hypothesis proposed in the preceding section, that TCP had a slightly higher affinity toward biochar than CTD due to its Langmuir constant value. However, in this case, this difference was starker than originally expected.

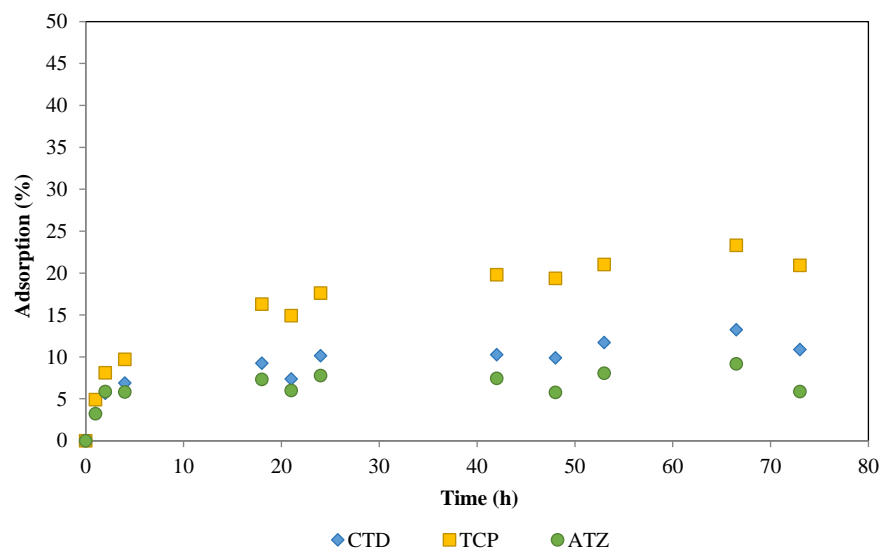


Figure 23. Adsorption profile of CTD, TCP and ATZ simultaneously on biochar with milli-Q water.

$[ATZ]_0 = [CTD]_0 = [TCP]_0 = 20 \mu\text{mol L}^{-1}$; $[BC]_0 = 50 \text{ mg L}^{-1}$; $T = 23^\circ\text{C}$; $\text{pH}_0 = 7.01$.

From these results, it can also be seen that the adsorption rate for any micropollutant was practically not higher than 25 %. This might be because the range of micromoles of pesticide per gram of biochar was too high, $400 \mu\text{mol g}^{-1}$ in this case, so there could be too many micromoles to adsorb for so little adsorbent.

By testing on the same water matrix (milli-Q water), but with much lower concentrations although still higher than the MP values found in water environments, a considerable change in adsorption efficiency was observed (see Figure 24).

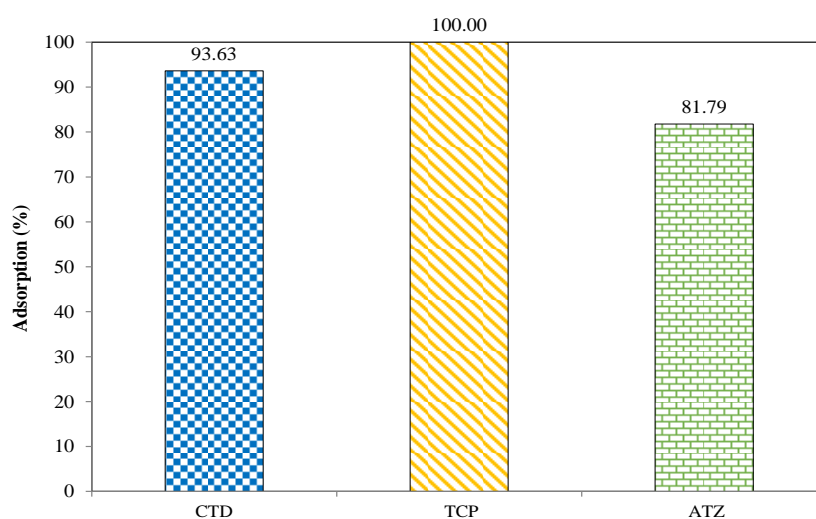


Figure 24. CTD, TCP and ATZ adsorption percentage achieved after 30h on biochar with milli-Q water.

$[ATZ]_0 = [CTD]_0 = [TCP]_0 = 2 \mu\text{mol L}^{-1}$; $[BC]_0 = 50 \text{ mg L}^{-1}$; $T = 22.8^\circ\text{C}$; $\text{pH}_0 = 7.01$

Within only 30 h, the TCP content of the solution had been entirely adsorbed on biochar, whereas for CTD and ATZ, the adsorption percentage achieved for each one was approximately 93.63 % and 81.79 %, respectively. These outcomes also reinforced the previous trend of the biochar preference for thiacloprid, followed by clothianidin and atrazine. In addition, this significant improvement in adsorption removal compared to the previous experiment was mainly due to the 90 % decrease in the pesticide-biochar ratio. In this case, this ratio was around $40 \mu\text{mol g}^{-1}$, so there were fewer adsorbate molecules for the same amount of adsorbent, therefore facilitating the adsorption process.

Finally, it was decided to assess the influence of the water matrix. Therefore, identical conditions as the previous experiment were replicated, but this time with a wastewater sample. As depicted in Figure 25, both clothianidin and thiacloprid followed a similar adsorption trend, achieving around 42-43 % of removal at 73 h. On the other hand, atrazine clearly showed the lowest adsorption capacity on biochar, as only $77.16 \mu\text{mol g}^{-1}$ were removed, which corresponded to about 23 % of adsorption.

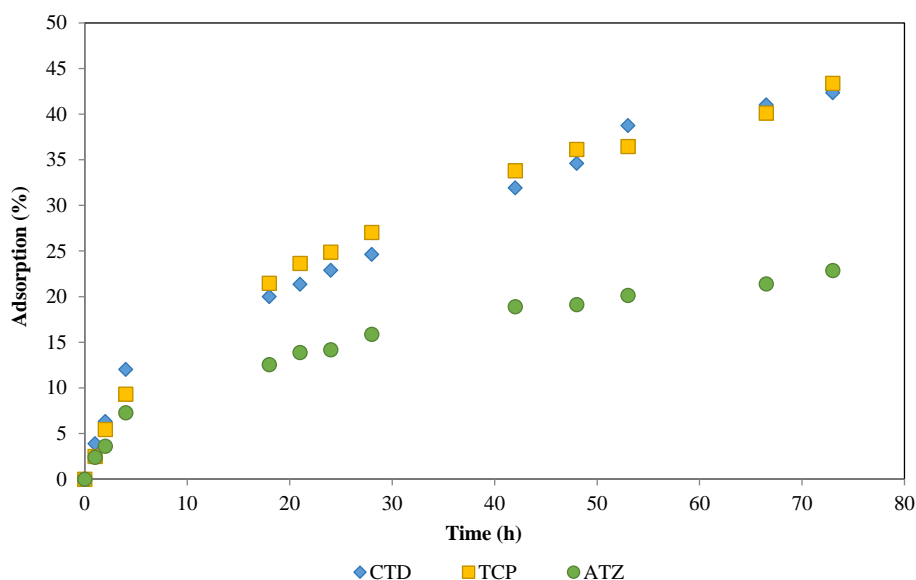


Figure 25. Adsorption profile of CTD, TCP and ATZ simultaneously on biochar with wastewater matrix. $[\text{ATZ}]_0 = [\text{CTD}]_0 = [\text{TCP}]_0 = 2 \mu\text{mol L}^{-1}$; $[\text{BC}]_0 = 50 \text{ mg L}^{-1}$; $T = 23.5^\circ\text{C}$; $\text{pH}_0 = 7.6$.

When these results were compared to the outcomes of the previous experiment, it could be noted that the water matrix had a considerable effect on the adsorption efficiency. Practically, more than 80 % or even total pesticide adsorption was achieved at 30 h with

the Milli-Q water matrix (see Figure 24), whereas for the same time, no more than 30 % of pesticide content was adsorbed with the wastewater matrix (see Figure 25).

From the different physicochemical parameters that characterised the real wastewater, it can be concluded, as expected, that wastewater is a more complex system than ultrapure water. The milli-Q water had a TOC value below $2 \mu\text{g L}^{-1}$ and did not present ions or turbidity. Therefore, no other compounds contained in the water matrix could interfere in the adsorption process and only the three pesticides were expected to be adsorbed on the biochar surface. In contrast, the wastewater matrix presented a higher TOC value (25 mg L^{-1}) and also nitrate/nitrite ions, among other characteristics (see Table 5). The presence of this dissolved and particulate organic matter in the solution could strongly compete with the target compounds for the different active sites of biochar, hindering thus the adsorption efficiency of these pesticides. In general, the different results achieved with each water matrix showed significant variations due, in part, to the presence of competing ions and organic matter.

Regarding the low adsorption capacity of atrazine onto biochar when compared to the other two neonicotinoids (see Figure 25), it could be affected, among other factors, by the presence of nitrate ions in the wastewater matrix. According to Xing et al. (2020), the removal efficiency of atrazine decreased considerably when NO_3^- ions were present in the solution, as they competed more, as explained above, with the target compound (atrazine) for occupying the active sites of biochar. In any case, the adsorption of atrazine was worse in all the situations analysed, so it was expected that in real water would act in the same way.

5. CONCLUSIONS

This work demonstrates that CO₂-physically activated biochar can be synthesised from rice husk, and despite its resultant characteristics, it can be employed as an adsorbent to remove these three concerning pesticides from wastewater effluents.

The biochar obtained from the carbonization stage at 500 °C for 4 h resulted in significantly alkaline (**10.73**), with a low surface area (**1.22 m² g⁻¹**) and high ash content (**36.28 %**). The CO₂-physical activation at 800 °C for 1 h provoked a complete change in its structure, as the ash content (**43.21 %**) and the surface area (**379.95 m² g⁻¹**) were considerably increased, whereas the elemental content of biochar declined significantly.

Pre-treating the feedstock with sodium carbonate proved to be ineffective to remove the silicon content. However, it was found that the Si-containing functional groups of biochar could play a key role and favour the adsorption process, tending towards the more hydrophilic compounds. This fact was confirmed by the results of studies carried out on each pesticide separately, as biochar followed the trend: **CTD > TCP > ATZ**.

Electrostatic interactions did not seem to be the main adsorption mechanism between pesticides-biochar. Furthermore, the pH effect did not strongly influence the ATZ and CTD adsorption, unlike TCP, which increased more than twice as much when moving from pH 2 (**109.92 μmol g⁻¹**) to pH 12 (**225.29 μmol g⁻¹**).

Assessment of adsorption isotherms revealed that ATZ adsorption on biochar seems to be reasonably well explained by the Freundlich model, whereas CTD and TCP were better described by the Langmuir model. It also indicated that the adsorption process was favourable, and that TCP had a higher affinity to biochar since it presented a greater Langmuir constant. This pattern was confirmed when all pesticides were tested simultaneously, as the adsorption biochar trend was **TCP > CTD > ATZ**.

Experiments with a real wastewater matrix showed lower adsorption capacity compared to the milli-Q water matrix one. This reduction was attributed to the competition and interference of organic matter and ions for the adsorption sites on the biochar.

6. FUTURE PERSPECTIVES

It should be noted that this work has been the start of a new line of research within the Advanced Oxidation Process Engineering group and it also received some advice and assistance from a group that had previously worked with biochars. It was performed at a lab-scale and, therefore, further experiments should be conducted in pilot-scale columns as fixed-bed adsorbers, to determine the feasibility of implementing it in the future as a tertiary treatment technology.

Furthermore, it would be interesting to try to synthesise this biochar, under the same conditions, but previously eliminate the large part of silicon contained originally. This would reveal how decisive or important the silicon content was in the adsorption process. Other activation methods, such as physical activation by steam or chemical acidification, could be assessed, as it would be interesting to determine how activation can affect the resulting properties.

Finally, as this line of work progress, it should attempt to develop new catalysts from iron-impregnated biochars, characterise them, and focus on assessing their catalytic activity in Fenton-oxidation reactions.

7. NOTATION

ACN	Acetonitrile
AC	Activated Carbon
AOP	Advanced Oxidation Process
ASTM	American Society for Testing and Materials
A _C	Ash content
ATZ	Atrazine
BJH	Barrett-Joyner-Halenda
BC	Biochar
BET	Brunauer-Emmett-Teller
CTD	Clothianidin
CEC	Contaminant of Emerging Concern
CAS	Conventional Activated Sludge
EC	Electrical Conductivity
EDA	Electron Donor-Acceptor
EPA	Environmental Protection Agency
EQS	Environmental Quality Standard
EU	European Union
FESEM	Field Emission Scanning Electron Microscopy
F _C	Fixed Carbon
FTIR	Fourier Transform Infrared
HPLC	High Performance Liquid Chromatography
IFAS	Integrated Fixed-Film Activated Sludge
IARC	International Agency for Research on Cancer
ISO	International Organization for Standardization
IUPAC	International Union of Pure and Applied Chemistry
MP	Micropollutant
M _C	Moisture Content
NN	Neonicotinoid
nAChR	Nicotinic Acetylcholine Receptor
pH _{PZC}	Point of Zero Charge
PS	Priority Substance

RH	Rice Husk
RHB	Rice Husk Biochar
R _L	Separation Faction
SSA	Specific Surface Area
SGD	Sustainable Development Goal
TCP	Thiacloprid
TOC	Total Organic Carbon
TSS	Total Suspended Solids
UPW	Ultrapure Water
UN	United Nations
UN-FAO	United Nations Food and Agriculture Organization
V _D	Volatile Matter
WWTP	Wastewater Treatment Plant
WL	Watch List
WFD	Water Framework Directive
WHO	World Health Organization
WWF	World Wildlife Fund

8. REFERENCES AND NOTES

- Ahiduzzaman, M., & Islam, A. K. M. S. (2016). Preparation of porous bio-char and activated carbon from rice husk by leaching ash and chemical activation. *SpringerPlus*.
<https://doi.org/10.1186/s40064-016-2932-8>
- Aldeguer Esquerdo, A., Sentana Gadea, I., Varo Galvañ, P. J., & Prats Rico, D. (2021). Efficacy of atrazine pesticide reduction in aqueous solution using activated carbon, ozone and a combination of both. *Science of the Total Environment*, 764.
<https://doi.org/10.1016/j.scitotenv.2020.144301>
- Ambaye, T. G., Vaccari, M., van Hullebusch, E. D., Amrane, A., & Rtimi, S. (2021). Mechanisms and adsorption capacities of biochar for the removal of organic and inorganic pollutants from industrial wastewater. *International Journal of Environmental Science and Technology*, 18(3), 3273–3294. <https://doi.org/10.1007/s13762-020-03060-w>
- APHA. (2005). *Standard Methods for the Examination of Water and Wastewater* (21st ed.).
- Asadi, H., Ghorbani, M., Rezaei-Rashti, M., Abrishamkesh, S., Amirahmadi, E., Chengrong, C., & Gorji, M. (2021). Application of Rice Husk Biochar for Achieving Sustainable Agriculture and Environment. In *Rice Science* (Vol. 28, Issue 4, pp. 325–343). Elsevier B.V.
<https://doi.org/10.1016/j.rsci.2021.05.004>
- Ayawei, N., Ebelegi, A. N., & Wankasi, D. (2017). Modelling and Interpretation of Adsorption Isotherms. In *Journal of Chemistry* (Vol. 2017). Hindawi Limited.
<https://doi.org/10.1155/2017/3039817>
- Barbosa, M. O., Moreira, N. F. F., Ribeiro, A. R., Pereira, M. F. R., & Silva, A. M. T. (2016). Occurrence and removal of organic micropollutants: An overview of the watch list of EU Decision 2015/495. In *Water Research* (Vol. 94, pp. 257–279). Elsevier Ltd.
<https://doi.org/10.1016/j.watres.2016.02.047>
- Binnal, P., Kumar, D. J., S P, M., & Patil, J. (2022). Upgrading the rice husk biochar characteristics through microwave assisted phosphoric acid pretreatment followed by coprolysis with LDPE. *Biofuels, Bioproducts and Biorefining*. <https://doi.org/10.1002/bbb.2392>
- CEFIC. (1986). *Test methods for activated carbon*.
- Chauhan, D. S., Quraishi, M. A., Nik, W. B. W., & Srivastava, V. (2021). Triazines as a potential class of corrosion inhibitors: Present scenario, challenges and future perspectives. In *Journal of Molecular Liquids* (Vol. 321). Elsevier B.V. <https://doi.org/10.1016/j.molliq.2020.114747>
- Chemerys, V., & Baltrėnaitė, E. (2016, April 7). *MODIFIED BIOCHAR: A REVIEW ON MODIFICATIONS OF BIOCHAR TOWARDS ITS ENHANCED ADSORPTIVE PROPERTIES*.
<https://doi.org/10.3846/aainz.2016.03>
- Choudhary, T. K., Khan, K. S., Hussain, Q., Ahmad, M., & Ashfaq, M. (2019). Feedstock-induced changes in composition and stability of biochar derived from different agricultural wastes. *Arabian Journal of Geosciences*, 12(20). <https://doi.org/10.1007/s12517-019-4735-z>
- Claoston, N., Samsuri, A. W., Ahmad Husni, M. H., & Mohd Amran, M. S. (2014). Effects of pyrolysis temperature on the physicochemical properties of empty fruit bunch and rice husk biochars. *Waste Management and Research*, 32(4), 331–339.
<https://doi.org/10.1177/0734242X14525822>
- Conte, P., Bertani, R., Sgarbossa, P., Bambina, P., Schmidt, H. P., Raga, R., lo Papa, G., Chillura Martino, D. F., & lo Meo, P. (2021). Recent developments in understanding biochar's physical–chemistry. In *Agronomy* (Vol. 11, Issue 4). MDPI AG.
<https://doi.org/10.3390/agronomy11040615>
- Cruz Alcalde, A. (2020). *Contribution to Performance Characterization and Kinetic Modelling of Micropollutants Abatement in Water and Wastewater by Ozone-based Oxidation Processes*.
www.tdx.cat
- Cruz-Alcalde, A., Sans, C., & Esplugas, S. (2017). Priority pesticides abatement by advanced water technologies: The case of acetamiprid removal by ozonation. *Science of the Total Environment*, 599–600, 1454–1461. <https://doi.org/10.1016/j.scitotenv.2017.05.065>
- de Albuquerque, F. P., de Oliveira, J. L., Moschini-Carlos, V., & Fraceto, L. F. (2020). An overview of the potential impacts of atrazine in aquatic environments: Perspectives for tailored solutions based on nanotechnology. *Science of The Total Environment*, 700, 134868.
<https://doi.org/10.1016/J.SCITOTENV.2019.134868>

- de Gisi, S., Lofrano, G., Grassi, M., & Notarnicola, M. (2016). Characteristics and adsorption capacities of low-cost sorbents for wastewater treatment: A review. In *Sustainable Materials and Technologies* (Vol. 9, pp. 10–40). Elsevier B.V. <https://doi.org/10.1016/j.susmat.2016.06.002>
- Depci, T. (2012). Comparison of activated carbon and iron impregnated activated carbon derived from Gölbaşı lignite to remove cyanide from water. *Chemical Engineering Journal*, 181–182, 467–478. <https://doi.org/10.1016/j.cej.2011.12.003>
- do Nascimento, C. T., Vieira, M. G. A., Scheufele, F. B., Palú, F., da Silva, E. A., & Borba, C. E. (2022). Adsorption of atrazine from aqueous systems on chemically activated biochar produced from corn straw. *Journal of Environmental Chemical Engineering*, 10(1). <https://doi.org/10.1016/j.jece.2021.107039>
- dos Santos, K. J. L., dos Santos, G. E. de S., de Sá, Í. M. G. L., Ide, A. H., Duarte, J. L. da S., de Carvalho, S. H. V., Soletti, J. I., & Meili, L. (2019). Wodyetia bifurcata biochar for methylene blue removal from aqueous matrix. *Bioresource Technology*, 293. <https://doi.org/10.1016/j.biortech.2019.122093>
- Dotto, G. L., & McKay, G. (2020). Current scenario and challenges in adsorption for water treatment. *Journal of Environmental Chemical Engineering*, 8(4). <https://doi.org/10.1016/j.jece.2020.103988>
- Eckhard Worch. (2012). *Eckhard Worch Adsorption Technology in Water Treatment*.
- El-Sayed, G. O., Yehia, M. M., & Asaad, A. A. (2014). Assessment of activated carbon prepared from corncob by chemical activation with phosphoric acid. *Water Resources and Industry*, 7–8, 66–75. <https://doi.org/10.1016/j.wri.2014.10.001>
- Enaime, G., Baçaoui, A., Yaacoubi, A., & Lübken, M. (2020). Biochar for wastewater treatment-conversion technologies and applications. In *Applied Sciences (Switzerland)* (Vol. 10, Issue 10). MDPI AG. <https://doi.org/10.3390/app10103492>
- European Commission. (2004). COMMISSION DECISION of 10 March 2004 concerning the non-inclusion of atrazine in Annex I to Council Directive 91/414/EEC and the withdrawal of authorisations for plant protection products containing this active substance. *OJ L* 78, 53–55.
- European Commission. (2018). COMMISSION IMPLEMENTING REGULATION (EU) 2018/784 of 29 May 2018 amending Implementing Regulation (EU) No 540/2011 as regards the conditions of approval of the active substance clothianidin. *OJ L* 132, 35–39. <https://doi.org/10.2903/j.efsa.2016.4606>
- European Commission. (2020). COMMISSION IMPLEMENTING REGULATION (EU) 2020/23 of 13 January 2020 concerning the non-renewal of the approval of the active substance thiacloprid, in accordance with Regulation (EC) No 1107/2009 of the European Parliament and of the Council concerning the placing of plant protection products on the market, and amending the Annex to Commission Implementing Regulation (EU) No 540/2011. *OJ L* 8, 8–11.
- FAO. (2022). *FAOSTAT*. <https://www.fao.org/faostat/en/#data/RP/visualize>
- Fidel, R. B., Laird, D. A., Thompson, M. L., & Lawrinenko, M. (2017). Characterization and quantification of biochar alkalinity. *Chemosphere*, 167, 367–373. <https://doi.org/10.1016/j.chemosphere.2016.09.151>
- Fierascu, I., Dima, S. O., Avramescu, S. M., Caloian, F., & Claudiu Fierascu, R. (2020). Facile Removal of Pesticides from Aqueous Solutions Using Magnetic Nanocomposites II. Adsorption experiments and kinetic study. In *REV.CHIM.(Bucharest)* ♦ (Vol. 71, Issue 1). <http://www.revistadechimie.ro>
- Foo, K. Y., & Hameed, B. H. (2010). Insights into the modeling of adsorption isotherm systems. In *Chemical Engineering Journal* (Vol. 156, Issue 1, pp. 2–10). <https://doi.org/10.1016/j.cej.2009.09.013>
- Girish, C. R., & Murty, V. R. (2016). Mass Transfer Studies on Adsorption of Phenol from Wastewater Using Lantana camara, Forest Waste. *International Journal of Chemical Engineering*, 2016. <https://doi.org/10.1155/2016/5809505>
- Gleick, P. H., & Cooley, H. (2021). *Annual Review of Environment and Resources Freshwater Scarcity*. <https://doi.org/10.1146/annurev-environ-012220>
- Goulson, D. (2013). *An overview of the environmental risks posed by neonicotinoid insecticides*. <https://doi.org/10.1111/1365-2664.12111>

- Gupta, M., Savla, N., Pandit, C., Pandit, S., Gupta, P. K., Pant, M., Khilari, S., Kumar, Y., Agarwal, D., Nair, R. R., Thomas, D., & Thakur, V. K. (2022). Use of biomass-derived biochar in wastewater treatment and power production: A promising solution for a sustainable environment. In *Science of the Total Environment* (Vol. 825). Elsevier B.V. <https://doi.org/10.1016/j.scitotenv.2022.153892>
- Gusmaroli, L., Buttiglieri, G., & Petrovic, M. (2019a). The EU watch list compounds in the Ebro delta region: Assessment of sources, river transport, and seasonal variations. *Environmental Pollution*, 253, 606–615. <https://doi.org/10.1016/j.envpol.2019.07.052>
- He, H., Liu, Y., You, S., Liu, J., Xiao, H., & Tu, Z. (2019). A review on recent treatment technology for herbicide atrazine in contaminated environment. In *International Journal of Environmental Research and Public Health* (Vol. 16, Issue 24). MDPI AG. <https://doi.org/10.3390/ijerph16245129>
- Huang, Z., Yuan, X., & Liu, X. (2021). The key drivers for the changes in global water scarcity: Water withdrawal versus water availability. *Journal of Hydrology*, 601. <https://doi.org/10.1016/j.jhydrol.2021.126658>
- Jiang, Z., Li, J., Jiang, D., Gao, Y., Chen, Y., Wang, W., Cao, B., Tao, Y., Wang, L., & Zhang, Y. (2020). Removal of atrazine by biochar-supported zero-valent iron catalyzed persulfate oxidation: Reactivity, radical production and transformation pathway. *Environmental Research*, 184, 109260. <https://doi.org/10.1016/j.envres.2020.109260>
- Jindo, K., Mizumoto, H., Sawada, Y., Sanchez-Monedero, M. A., & Sonoki, T. (2014). Physical and chemical characterizations of biochars derived from different agricultural residues. *Biogeosciences Discuss*, 11, 11727–11746. <https://doi.org/10.5194/bgd-11-11727-2014>
- Jongpradist, P., Homtragoon, W., Sukkarak, R., Kongkitkul, W., & Jamsawang, P. (2018). Efficiency of Rice Husk Ash as Cementitious Material in High-Strength Cement-Admixed Clay. <https://doi.org/10.1155/2018/8346319>
- Jung, S. H., & Kim, J. S. (2014). Production of biochars by intermediate pyrolysis and activated carbons from oak by three activation methods using CO₂. *Journal of Analytical and Applied Pyrolysis*, 107, 116–122. <https://doi.org/10.1016/j.jaap.2014.02.011>
- Jurado, A., Walther, M., & Díaz-Cruz, M. S. (2019). Occurrence, fate and environmental risk assessment of the organic microcontaminants included in the Watch Lists set by EU Decisions 2015/495 and 2018/840 in the groundwater of Spain. In *Science of the Total Environment* (Vol. 663, pp. 285–296). Elsevier B.V. <https://doi.org/10.1016/j.scitotenv.2019.01.270>
- Justo Llopis, A. (2015). *Advanced technologies applied to wastewater treatment plant effluents*.
- Kah, M., Sigmund, G., Xiao, F., & Hofmann, T. (2017). Sorption of ionizable and ionic organic compounds to biochar, activated carbon and other carbonaceous materials. In *Water Research* (Vol. 124, pp. 673–692). Elsevier Ltd. <https://doi.org/10.1016/j.watres.2017.07.070>
- Kozyatnyk, I., Oesterle, P., Wurzer, C., Mašek, O., & Jansson, S. (2021). Removal of contaminants of emerging concern from multicomponent systems using carbon dioxide activated biochar from lignocellulosic feedstocks. *Bioresource Technology*, 340. <https://doi.org/10.1016/j.biortech.2021.125561>
- Krasucka, P., Pan, B., Sik Ok, Y., Mohan, D., Sarkar, B., & Oleszczuk, P. (2021). Engineered biochar – A sustainable solution for the removal of antibiotics from water. *Chemical Engineering Journal*, 405, 126926. <https://doi.org/10.1016/j.cej.2020.126926>
- Li, Y., Su, P., Li, Y., Wen, K., Bi, G., & Cox, M. (2018). Adsorption-desorption and degradation of insecticides clothianidin and thiamethoxam in agricultural soils. *Chemosphere*, 207, 708–714. <https://doi.org/10.1016/j.chemosphere.2018.05.139>
- Liang, Z., Mahmoud Abdelshafy, A., Luo, Z., Belwal, T., Lin, X., Xu, Y., Wang, L., Yang, M., Qi, M., Dong, Y., & Li, L. (2022). Occurrence, detection, and dissipation of pesticide residue in plant-derived foodstuff: A state-of-the-art review. In *Food Chemistry* (Vol. 384). Elsevier Ltd. <https://doi.org/10.1016/j.foodchem.2022.132494>
- Limousin, G., Gaudet, J. P., Charlet, L., Szenknect, S., Barthès, V., & Krimissa, M. (2007). Sorption isotherms: A review on physical bases, modeling and measurement. In *Applied Geochemistry* (Vol. 22, Issue 2, pp. 249–275). Elsevier Ltd. <https://doi.org/10.1016/j.apgeochem.2006.09.010>
- López-Vinent, N., Cruz-Alcalde, A., Giménez, J., & Esplugas, S. (2021). Mixtures of chelating agents to enhance photo-Fenton process at natural pH: Influence of wastewater matrix on

- micropollutant removal and bacterial inactivation. *Science of the Total Environment*, 786. <https://doi.org/10.1016/j.scitotenv.2021.147416>
- Luo, Y., Guo, W., Ngo, H. H., Nghiem, L. D., Hai, F. I., Zhang, J., Liang, S., & Wang, X. C. (2014). A review on the occurrence of micropollutants in the aquatic environment and their fate and removal during wastewater treatment. In *Science of the Total Environment* (Vols. 473–474, pp. 619–641). Elsevier B.V. <https://doi.org/10.1016/j.scitotenv.2013.12.065>
- Manousi, N., Kabir, A., & Zachariadis, G. A. (2022). Recent advances in the extraction of triazine herbicides from water samples. In *Journal of Separation Science* (Vol. 45, Issue 1, pp. 113–133). John Wiley and Sons Inc. <https://doi.org/10.1002/jssc.202100313>
- Meiirkhanuly, Z., Koziel, J. A., Białowiec, A., Banik, C., & Brown, R. C. (2019). The-proof-of-concept of biochar floating cover influence on water pH. *Water (Switzerland)*, 11(9). <https://doi.org/10.3390/w11091802>
- Mondol, M. M. H., & Jhung, S. H. (2021). Adsorptive removal of pesticides from water with metal–organic framework-based materials. In *Chemical Engineering Journal* (Vol. 421). Elsevier B.V. <https://doi.org/10.1016/j.cej.2021.129688>
- Morales, L. F., Herrera, K., López, J. E., & Saldarriaga, J. F. (2021). Use of biochar from rice husk pyrolysis: assessment of reactivity in lime pastes. *Heliyon*, 7(11). <https://doi.org/10.1016/j.heliyon.2021.e08423>
- Morcali, M. H., Zeytuncu, B., & Yucel, O. (2013). Platinum uptake from chloride solutions using biosorbents. *Materials Research*, 16(2), 528–538. <https://doi.org/10.1590/S1516-14392013005000006>
- Nageeb, M. (2013). Adsorption Technique for the Removal of Organic Pollutants from Water and Wastewater. In *Organic Pollutants - Monitoring, Risk and Treatment*. InTech. <https://doi.org/10.5772/54048>
- Naumann, T., Bento, C. P. M., Wittmann, A., Gandrass, J., Tang, J., Zhen, X., Liu, L., & Ebinghaus, R. (2022a). Occurrence and ecological risk assessment of neonicotinoids and related insecticides in the Bohai Sea and its surrounding rivers, China. *Water Research*, 209. <https://doi.org/10.1016/j.watres.2021.117912>
- Nidheesh, P. v., Gopinath, A., Ranjith, N., Praveen Akre, A., Sreedharan, V., & Suresh Kumar, M. (2021). Potential role of biochar in advanced oxidation processes: A sustainable approach. In *Chemical Engineering Journal* (Vol. 405). Elsevier B.V. <https://doi.org/10.1016/j.cej.2020.126582>
- Nurul Farhana, A., Alias, A. B., Talib, N., Abd Rashid, Z., & Ghani, W. A. W. A. K. (2018). Characteristics of rice husk biochar blended with coal fly ash for potential sorption material. *Malaysian Journal of Analytical Sciences*, 22(2), 326–332. <https://doi.org/10.17576/mjas-2018-2202-19>
- Park, W., Kim, H., Park, H., Choi, S., Hong, S. J., & Bahk, Y.-M. (2021). Biochar as a low-cost, eco-friendly, and electrically conductive material for terahertz applications. *Scientific Reports*, 11, 18498. <https://doi.org/10.1038/s41598-021-98009-5>
- Pesqueira, J. F. J. R., Pereira, M. F. R., & Silva, A. M. T. (2020). Environmental impact assessment of advanced urban wastewater treatment technologies for the removal of priority substances and contaminants of emerging concern: A review. In *Journal of Cleaner Production* (Vol. 261). Elsevier Ltd. <https://doi.org/10.1016/j.jclepro.2020.121078>
- Phan, K. A., Phihusut, D., & Tuntiwiwattanapun, N. (2022). Preparation of rice husk hydrochar as an atrazine adsorbent: Optimization, characterization, and adsorption mechanisms. *Journal of Environmental Chemical Engineering*, 10(3), 107575. <https://doi.org/10.1016/j.jece.2022.107575>
- Phuong, D., Miyanishi, T., Okayama, T., & Kose, R. (2016). PORE STRUCTURE & ADSORPTION PROPERTIES OF BIOCHARS DERIVED FROM RICE RESIDUES AS AFFECTED BY VARIETY AND PYROLYSIS TEMPERATURE. *American Journal of Innovative Research and Applied Sciences*, 2(5), 179–189.
- Piccin, J. S., Dotto, G. L., & Pinto, L. A. A. (2011). Adsorption isotherms and thermochemical data of FDandC RED N° 40 Binding by chitosan. *Brazilian Journal of Chemical Engineering*, 28(2), 295–304. <https://doi.org/10.1590/S0104-66322011000200014>
- Pietrzak, D., Kania, J., Kmiecik, E., Malina, G., & Wątor, K. (2020). Fate of selected neonicotinoid insecticides in soil–water systems: Current state of the art and knowledge gaps. *Chemosphere*, 255. <https://doi.org/10.1016/j.chemosphere.2020.126981>

- Ponnuchamy, M., Kapoor, A., Ponnusamy, ., Kumar, S., Dai-Viet, ., Vo, N., Balakrishnan, A., Meenu, ., Jacob, M., & Sivaraman, . Prabhakar. (2021). *Sustainable adsorbents for the removal of pesticides from water: a review*. 19, 2425–2463. <https://doi.org/10.1007/s10311-021-01183-1>
- Porada, S., Zhao, R., van der Wal, A., Presser, V., & Biesheuvel, P. M. (2013). Review on the science and technology of water desalination by capacitive deionization. In *Progress in Materials Science* (Vol. 58, Issue 8, pp. 1388–1442). Elsevier Ltd. <https://doi.org/10.1016/j.pmatsci.2013.03.005>
- Qiu, B., Tao, X., Wang, H., Li, W., Ding, X., & Chu, H. (2021). Biochar as a low-cost adsorbent for aqueous heavy metal removal: A review. In *Journal of Analytical and Applied Pyrolysis* (Vol. 155). Elsevier B.V. <https://doi.org/10.1016/j.jaap.2021.105081>
- Rafiei-Sardooi, E., Azareh, A., Joorabian Shooshtari, S., & Parteli, E. J. R. (2022). Long-term assessment of land-use and climate change on water scarcity in an arid basin in Iran. *Ecological Modelling*, 467, 109934. <https://doi.org/10.1016/j.ecolmodel.2022.109934>
- Rápó, E., & Tonk, S. (2017). *Factors Affecting Synthetic Dye Adsorption; Desorption Studies: A Review of Results from the Last Five Years (2017-2021)*. 26, 5419. <https://doi.org/10.3390/molecules26175419>
- Rathi, B. S., & Kumar, P. S. (2021). Application of adsorption process for effective removal of emerging contaminants from water and wastewater. *Environmental Pollution*, 280. <https://doi.org/10.1016/j.envpol.2021.116995>
- Rezende-Teixeira, P., Dusi, R. G., Jimenez, P. C., Espindola, L. S., & Costa-Lotufo, L. v. (2022). What can we learn from commercial insecticides? Efficacy, toxicity, environmental impacts, and future developments. In *Environmental Pollution* (Vol. 300). Elsevier Ltd. <https://doi.org/10.1016/j.envpol.2022.118983>
- Saha, A., Gajbhiye, V. T., Gupta, S., Kumar, R., & Ghosh, R. K. (2014). Simultaneous Removal of Pesticides from Water by Rice Husk Ash: Batch and Column Studies. *Water Environment Research*, 86(11), 2176–2185. <https://doi.org/10.2175/106143014x14062131178358>
- Sahoo, D., & Remya, N. (2020). *Influence of operating parameters on the microwave pyrolysis of rice husk: biochar yield, energy yield, and property of biochar*. <https://doi.org/10.1007/s13399-020-00914-8>
- Saleh, I. A., Zouari, N., & Al-Ghouti, M. A. (2020). Removal of pesticides from water and wastewater: Chemical, physical and biological treatment approaches. In *Environmental Technology and Innovation* (Vol. 19). Elsevier B.V. <https://doi.org/10.1016/j.eti.2020.101026>
- Salman, J. M., Njoku, V. O., & Hameed, B. H. (2011). Adsorption of pesticides from aqueous solution onto banana stalk activated carbon. *Chemical Engineering Journal*, 174(1), 41–48. <https://doi.org/10.1016/j.cej.2011.08.026>
- Salomón, Y. L., Georgin, J., Franco, D. S. P., Netto, M. S., Piccilli, D. G. A., Foletto, E. L., Pinto, D., Oliveira, M. L. S., & Dotto, G. L. (2022). Adsorption of atrazine herbicide from water by diospyros kaki fruit waste activated carbon. *Journal of Molecular Liquids*, 347. <https://doi.org/10.1016/j.molliq.2021.117990>
- Semren, T. Ž., Žunec, S., & Pizent, A. (2018). Oxidative stress in triazine pesticide toxicity: A review of the main biomarker findings. In *Arhiv za Higijenu Rada i Toksikologiju* (Vol. 69, Issue 2, pp. 109–125). Sciendo. <https://doi.org/10.2478/aiht-2018-69-3118>
- Serrano, E., Munoz, M., de Pedro, Z. M., & Casas, J. A. (2019). Efficient removal of the pharmaceutical pollutants included in the EU Watch List (Decision 2015/495) by modified magnetite/H₂O₂. *Chemical Engineering Journal*, 376. <https://doi.org/10.1016/j.cej.2018.10.202>
- Sgolastra, F., Medrzycki, P., Bortolotti, L., Maini, S., Porrini, C., Simon-Delso, N., & Bosch, J. (2020). Bees and pesticide regulation: Lessons from the neonicotinoid experience. *Biological Conservation*, 241. <https://doi.org/10.1016/j.biocon.2019.108356>
- Sharifi, N., Nasiri, A., Silva Martínez, S., & Amiri, H. (2022). Synthesis of Fe₃O₄@activated carbon to treat metronidazole effluents by adsorption and heterogeneous Fenton with effluent bioassay. *Journal of Photochemistry and Photobiology A: Chemistry*, 427, 113845. <https://doi.org/10.1016/j.jphotochem.2022.113845>
- Shi, J., Fan, X., Tsang, D. C. W., Wang, F., Shen, Z., Hou, D., & Alessi, D. S. (2019). Removal of lead by rice husk biochars produced at different temperatures and implications for their

- environmental utilizations. *Chemosphere*, 235, 825–831.
<https://doi.org/10.1016/j.chemosphere.2019.06.237>
- Singh, B., Shen, Q., Arbestain, M. C., Dolk, M. M., & Camps-Arbestain, M. (2017). Biochar pH, electrical conductivity and liming potential. In B. Singh, M. Camps-Arbestain, & J. Lehmann (Eds.), *Biochar: A Guide to Analytical Methods* (pp. 23–38). CSIRO.
<https://www.researchgate.net/publication/319206365>
- Singh Karam, D., Nagabovanalli, P., Sundara Rajoo, K., Fauziah Ishak, C., Abdu, A., Rosli, Z., Melissa Muharam, F., & Zulperi, D. (2021). An overview on the preparation of rice husk biochar, factors affecting its properties, and its agriculture application. In *Journal of the Saudi Society of Agricultural Sciences*. King Saud University.
<https://doi.org/10.1016/j.jssas.2021.07.005>
- Sousa, J. C. G., Ribeiro, A. R., Barbosa, M. O., Ribeiro, C., Tiritan, M. E., Pereira, M. F. R., & Silva, A. M. T. (2019). Monitoring of the 17 EU Watch List contaminants of emerging concern in the Ave and the Sousa Rivers. *Science of the Total Environment*, 649, 1083–1095.
<https://doi.org/10.1016/j.scitotenv.2018.08.309>
- Steffens, C., Ballen, S. C., Scapin, E., da Silva, D. M., Steffens, J., & Jacques, R. A. (2022). Advances of nanobiosensors and its application in atrazine detection in water: A review. *Sensors and Actuators Reports*, 4, 100096. <https://doi.org/10.1016/J.SNR.2022.100096>
- Stephanie, H., Mlsna, T. E., & Wipf, D. O. (2021). Functionalized biochar electrodes for asymmetrical capacitive deionization. *Desalination*, 516.
<https://doi.org/10.1016/j.desal.2021.115240>
- Tan, X. fei, Liu, S. bo, Liu, Y. guo, Gu, Y. ling, Zeng, G. ming, Hu, X. jiang, Wang, X., Liu, S. heng, & Jiang, L. hua. (2017). Biochar as potential sustainable precursors for activated carbon production: Multiple applications in environmental protection and energy storage. In *Bioresource Technology* (Vol. 227, pp. 359–372). Elsevier Ltd.
<https://doi.org/10.1016/j.biortech.2016.12.083>
- Tiedeken, E. J., Tahar, A., McHugh, B., & Rowan, N. J. (2017). Monitoring, sources, receptors, and control measures for three European Union watch list substances of emerging concern in receiving waters – A 20 year systematic review. In *Science of the Total Environment* (Vol. 574, pp. 1140–1163). Elsevier B.V. <https://doi.org/10.1016/j.scitotenv.2016.09.084>
- Tomczyk, A., Sokołowska, Z., & Boguta, P. (2020). Biochar physicochemical properties: pyrolysis temperature and feedstock kind effects. In *Reviews in Environmental Science and Biotechnology* (Vol. 19, Issue 1, pp. 191–215). Springer. <https://doi.org/10.1007/s11157-020-09523-3>
- Tran, H. N., You, S. J., Hosseini-Bandegharaei, A., & Chao, H. P. (2017). Mistakes and inconsistencies regarding adsorption of contaminants from aqueous solutions: A critical review. In *Water Research* (Vol. 120, pp. 88–116). Elsevier Ltd.
<https://doi.org/10.1016/j.watres.2017.04.014>
- Tran, V. S., Ngo, H. H., Guo, W., Zhang, J., Liang, S., Ton-That, C., & Zhang, X. (2015). Typical low cost biosorbents for adsorptive removal of specific organic pollutants from water. In *Bioresource Technology* (Vol. 182, pp. 353–363). Elsevier Ltd.
<https://doi.org/10.1016/j.biortech.2015.02.003>
- UN General Assembly. (n.d.). *Target 6.3 – Water quality and wastewater - sdg6monitoring*. Retrieved March 13, 2022, from <https://www.sdg6monitoring.org/indicators/target-63/>
- Varjani, S., Kumar, G., & Rene, E. R. (2019). Developments in biochar application for pesticide remediation: Current knowledge and future research directions. *Journal of Environmental Management*, 232, 505–513. <https://doi.org/10.1016/j.jenvman.2018.11.043>
- Vinayagam, V., Murugan, S., Kumaresan, R., Narayanan, M., Sillanpää, M., Viet N Vo, D., Kushwaha, O. S., Jenis, P., Potdar, P., & Gadiya, S. (2022). Sustainable adsorbents for the removal of pharmaceuticals from wastewater: A review. *Chemosphere*, 300, 134597.
<https://doi.org/10.1016/j.chemosphere.2022.134597>
- Wang, C. (2021). Production of biochar from renewable resources. In *Advanced Technology for the Conversion of Waste into Fuels and Chemicals* (pp. 273–287). Elsevier.
<https://doi.org/10.1016/b978-0-12-823139-5.00018-6>
- Wang, R. Z., Huang, D. L., Liu, Y. G., Zhang, C., Lai, C., Wang, X., Zeng, G. M., Gong, X. M., Duan, A., Zhang, Q., & Xu, P. (2019). Recent advances in biochar-based catalysts: Properties,

- applications and mechanisms for pollution remediation. In *Chemical Engineering Journal* (Vol. 371, pp. 380–403). Elsevier B.V. <https://doi.org/10.1016/j.cej.2019.04.071>
- Wang, X., Guo, Z., Hu, Z., & Zhang, J. (2020). Recent advances in biochar application for water and wastewater treatment: A review. In *PeerJ* (Vol. 8). PeerJ Inc. <https://doi.org/10.7717/peerj.9164>
- Weisner, O., Arle, J., Liebmann, L., Link, M., Schäfer, R. B., Schneeweiss, A., Schreiner, V. C., Vormeier, P., & Liess, M. (2022). Three reasons why the Water Framework Directive (WFD) fails to identify pesticide risks. *Water Research*, 208. <https://doi.org/10.1016/j.watres.2021.117848>
- Xiao, F., & Pignatello, J. J. (2015). Interactions of triazine herbicides with biochar: Steric and electronic effects. *Water Research*, 80, 179–188. <https://doi.org/10.1016/j.watres.2015.04.040>
- Xing, R., He, J., Hao, P., & Zhou, W. (2020). Graphene oxide-supported nanoscale zero-valent iron composites for the removal of atrazine from aqueous solution. *Colloids and Surfaces A: Physicochemical and Engineering Aspects*, 589. <https://doi.org/10.1016/j.colsurfa.2020.124466>
- Xu, Z., He, M., Xu, X., Cao, X., & Tsang, D. C. W. (2021). Impacts of different activation processes on the carbon stability of biochar for oxidation resistance. *Bioresource Technology*, 338. <https://doi.org/10.1016/j.biortech.2021.125555>
- Yang, S., He, L., Peng, P., Liu, Y., Ma, Y., Wu, L., Zhang, Z., & Yang, L. (2022). Synergistic Fe²⁺/UV activated peroxydisulfate as an efficient method for the degradation of thiacloprid. *Process Safety and Environmental Protection*, 161, 466–475. <https://doi.org/10.1016/j.psep.2022.03.061>
- Yavari, S., Malakahmad, A., Sapari, N. B., & Yavari, S. (2017). Sorption properties optimization of agricultural wastes-derived biochars using response surface methodology. *Process Safety and Environmental Protection*, 109, 509–519. <https://doi.org/10.1016/j.psep.2017.05.002>
- Yousef, R., Qiblawey, H., & El-Naas, M. H. (2020). Adsorption as a process for produced water treatment: A review. In *Processes* (Vol. 8, Issue 12, pp. 1–22). MDPI AG. <https://doi.org/10.3390/pr8121657>
- Zhang, C., Li, F., Wen, R., Zhang, H., Elumalai, P., Zheng, Q., Chen, H., Yang, Y., Huang, M., & Ying, G. (2020). Heterogeneous electro-Fenton using three-dimension NZVI-BC electrodes for degradation of neonicotinoid wastewater. *Water Research*, 182, 115975. <https://doi.org/10.1016/j.watres.2020.115975>
- Zhang, P., Ren, C., Sun, H., & Min, L. (2018). Sorption, desorption and degradation of neonicotinoids in four agricultural soils and their effects on soil microorganisms. *Science of the Total Environment*, 615, 59–69. <https://doi.org/10.1016/j.scitotenv.2017.09.097>
- Zhang, P., Sun, H., Ren, C., Min, L., & Zhang, H. (2018). Sorption mechanisms of neonicotinoids on biochars and the impact of deashing treatments on biochar structure and neonicotinoids sorption. *Environmental Pollution*, 234, 812–820. <https://doi.org/10.1016/j.envpol.2017.12.013>
- Zulkania, A., Hanum, G. F., & Sri Rezki, A. (2018). The potential of activated carbon derived from bio-char waste of bio-oil pyrolysis as adsorbent. *MATEC Web of Conferences*, 154. <https://doi.org/10.1051/mateconf/201815401029>

APPENDIX

APP 1: ADSORPTION PROFILES OF PRELIMINARY EXPERIMENTS

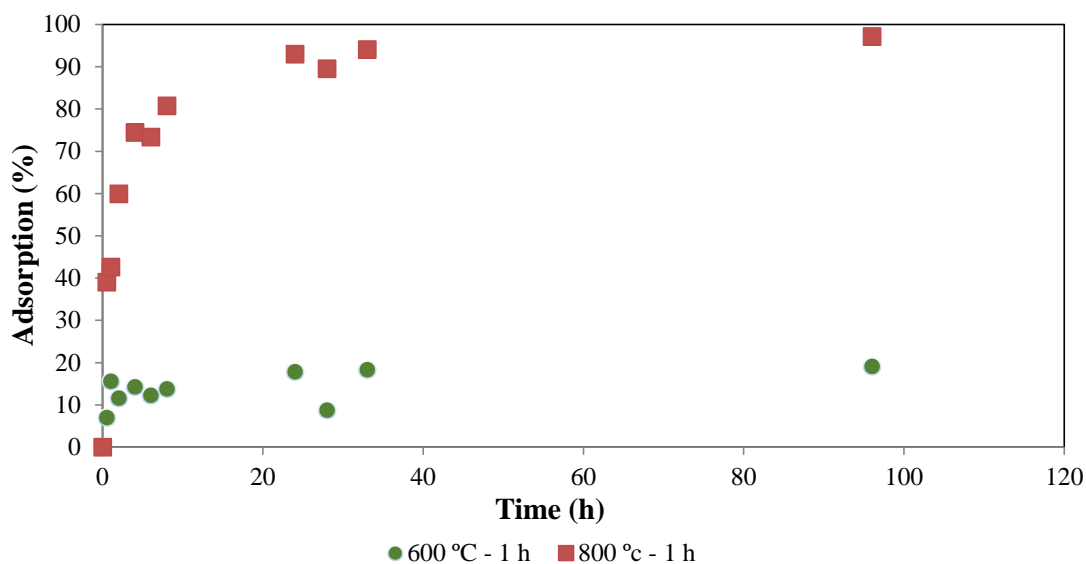


Figure A1. Adsorption profile of CTD on biochar from rice husk (100 μm) pyrolyzed at 500 °C for 4 h at different activation temperatures. $[CTD]_0 = 0.1 \text{ mg L}^{-1}$; $[BC] = 500 \text{ mg L}^{-1}$; $T = 22.3 \text{ }^\circ\text{C}$

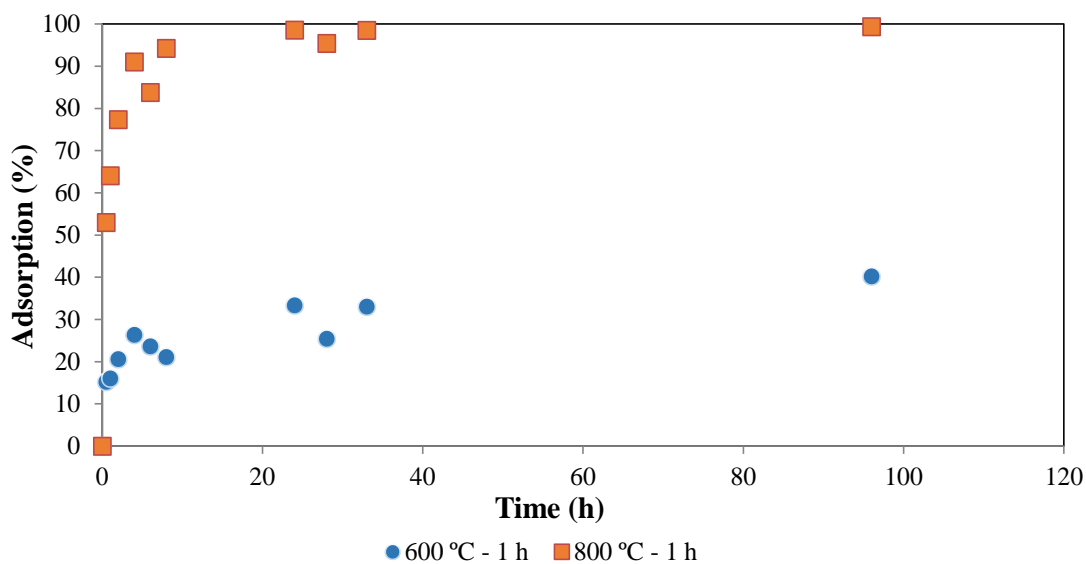


Figure A2. Adsorption profile of CTD on biochar from rice husk (100 μm) pyrolyzed at 700 °C for 4 h at different activation temperatures. $[CTD]_0 = 0.1 \text{ mg L}^{-1}$; $[BC] = 500 \text{ mg L}^{-1}$; $T = 22.5 \text{ }^\circ\text{C}$

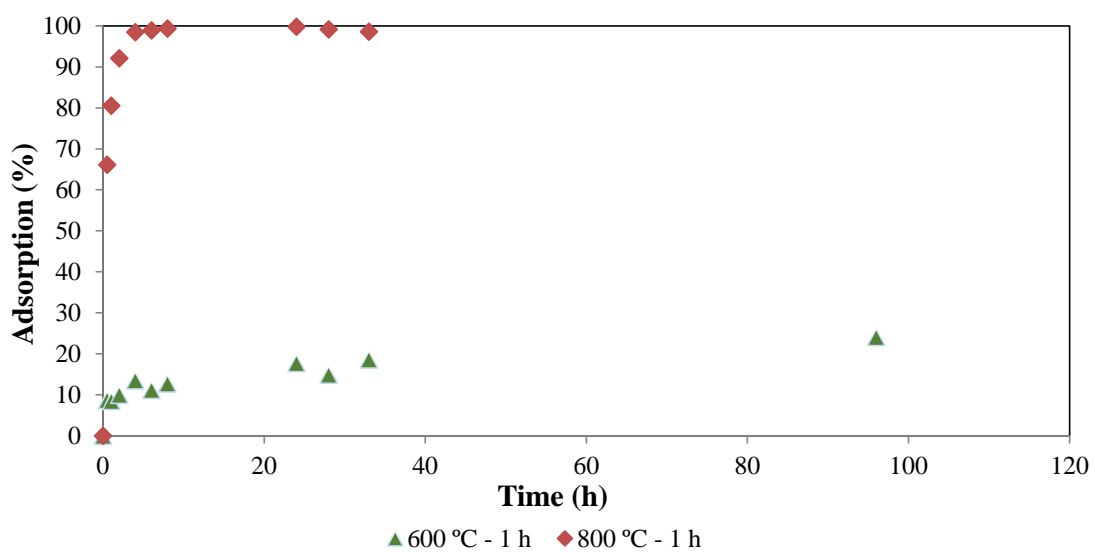


Figure A3. Adsorption profile of CTD on biochar from rice husk (250 μm) pyrolyzed at 500 $^{\circ}\text{C}$ for 4 h at different activation temperatures. $[\text{CTD}]_0 = 0.1 \text{ mg L}^{-1}$; $[\text{BC}] = 500 \text{ mg L}^{-1}$; $T = 22.3 \text{ }^{\circ}\text{C}$

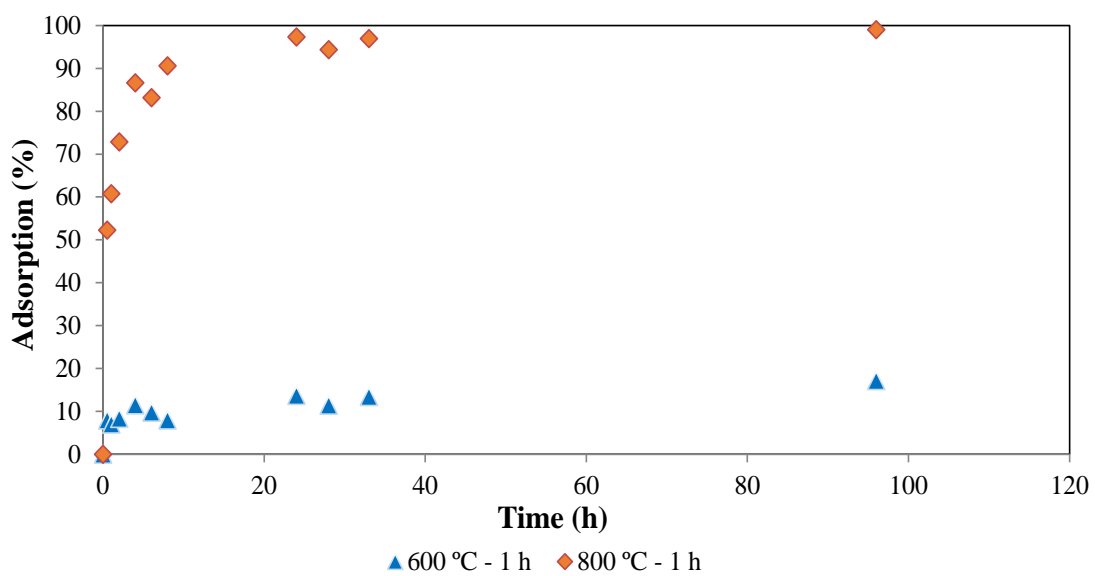


Figure A4. Adsorption profile of CTD on biochar from rice husk (250 μm) pyrolyzed at 700 $^{\circ}\text{C}$ for 4 h at different activation temperatures. $[\text{CTD}]_0 = 0.1 \text{ mg L}^{-1}$; $[\text{BC}] = 500 \text{ mg L}^{-1}$; $T = 22.3 \text{ }^{\circ}\text{C}$